chemosensors

MDPI

Review

The Photoluminescence and Biocompatibility of $CuInS_2$-Based Ternary Quantum Dots and Their Biological Applications

Rajendran Jose Varghese [1,2] and Oluwatobi Samuel Oluwafemi [1,2,*]

[1] Department of Chemical Sciences, University of Johannesburg, P.O. Box 17011, Doornfontein, Johannesburg 2028, South Africa; 201613568@student.uj.ac.za

[2] Centre for Nanomaterials Science Research, University of Johannesburg, P.O. Box 17011, Doornfontein, Johannesburg 2028, South Africa

* Correspondence: oluwafemi.oluwatobi@gmail.com

Received: 2 September 2020; Accepted: 2 October 2020; Published: 15 October 2020

Abstract: Semiconductor quantum dots (QDs) have become a unique class of materials with great potential for applications in biomedical and optoelectronic devices. However, conventional QDs contains toxic heavy metals such as Pb, Cd and Hg. Hence, it is imperative to find an alternative material with similar optical properties and low cytotoxicity. Among these materials, $CuInS_2$ (CIS) QDs have attracted a lot of interest due to their direct band gap in the infrared region, large optical absorption coefficient and low toxic composition. These factors make them a good material for biomedical application. This review starts with the origin and photophysical characteristics of CIS QDs. This is followed by various synthetic strategies, including synthesis in organic and aqueous solvents, and the tuning of their optical properties. Lastly, their significance in various biological applications is presented with their prospects in clinical applications.

Keywords: $CuInS_2$ quantum dots; optical materials; cytotoxicity; bioimaging

1. Introduction

Semiconductor nanoparticles, also referred to as zero-dimensional material or quantum dots (QDs), have gained significant interest in many areas of applications ranging from water to energy, sensing and biological applications due to their quantum confinement effect [1–4]. Compared to conventional organic dyes, QDs exhibit high photostability and tunable optical properties by changing the size and composition [5]. The development/research on binary QDs has received considerable interest, and the field has been explored extensively; however, only a few commercial products have been developed due to their toxic composition [6]. Therefore, alternative, low or non-toxic material is imperative, especially for biological application [7–10]. The II-VI group and IV-VI group-based materials have been extensively studied, while other materials such as binary III-V and low-toxic ternary I-III-VI are less explored [11]. The I-III-VI quantum dots, which contain group I (Cu, Ag), group III (Al, Ga, In, Ti) and group IV (S, Se, Te), have been reported as less toxic compared to II-VI binary QDs. The replacement of group II in II-VI binary QDs by group I and group III cations has led to the production of Cd- and Pb-free ternary nanocrystals NCs/QDs (e.g., $CuInS_2$, $AgInS_2$).

The basic synthetic method for the formation of ternary QDs is based on the initial formation of nuclei, which are combined to form multinary NCs, or through the nuclei, which can also act as seeds and facilitate cation exchange or ionic diffusion [9,12]. For example, binary copper chalcogenides (e.g., Cu_2S) can be subjected to a partial cationic exchange which can partly replace copper ions with other cations (e.g., Zn^{2+}, Sn^{4+}) [13]. The limitation of this method is the long reaction times

and polydispersity. Therefore, to obtain a monodisperse confined NCs with controlled composition, the cationic reaction should be finely balanced. Thus, using stabilizing agents to control the reactivity of the precursors has been proposed [14–18]. In order to tune the optical properties of the ternary NCs, the control on composition and phase homogeneities are very important. The desired phase of the crystal depends on the nature of cation and control on the site occupancy by tuning the precursors, surfactant and experimental conditions (Figure 1). $CuInS_2$ (CIS) is a direct semiconductor with a bandgap of around 1.45 eV, a large extinction coefficient, good radiation hardness and excellent defect tolerance. The Bohr exciton radius of CIS NCs is reported to be around 4.1 nm, and the quantum confinement in this crystal can be observed until it reaches 8 nm in diameter [19]. There are reports on the tuning of its emission position as the diameter of the CIS changes [20,21] but with a broad full width and half maxima (FWHM) (90–120 nm) compared to binary QDs. The initial assessment of this broadness was focused on the size distribution of the as-synthesized material [20]. However, after various reports, this broadness of photoluminescence (PL) spectra has been shown to be independent of the size distribution in the case of CIS-based QDs and can be attributed to the distribution of vibrational states [21,22]. This shows that quantum size effects are not the only factors that can influence the bandgap of the ternary NCs [7,20,22], as the composition of anions and cations also plays a major factor [23,24]. Regarding the composition tuning, the valence band of the CIS (Cu 3d and S 3p orbital) can be lowered when the Cu content is reduced. The tuning of composition leads to the stoichiometric deviation, which, in turn, generates a large number of donor–acceptor states within the bandgap. These high densities of states lead to a high probability of radiative recombination of donor–acceptor and result in broad photoluminescence (PL) spectra, long PL lifetime and a shift in stokes [10,25]. The time-resolved PL (TRPL) analysis is used to understand the charge recombination in these QDs. For the ternary QDs, the PL decay is usually reported to be double/triple exponential analysis. The average PL lifetime for CIS QDs is reported to be between 100–300 ns, which is much longer than the binary QDs. As reported, the PL decay also depends on the composition of the CIS NCs [21]. Thus, the bandgap cannot be determined by merely accessing the PL spectra. Moreover, the large volumes of defects lower the quantum yield (QY). From this, we can conclude that the optical property of ternary QDs depends not only on the size but also on the composition, crystal phase, ordering and surface passivation.

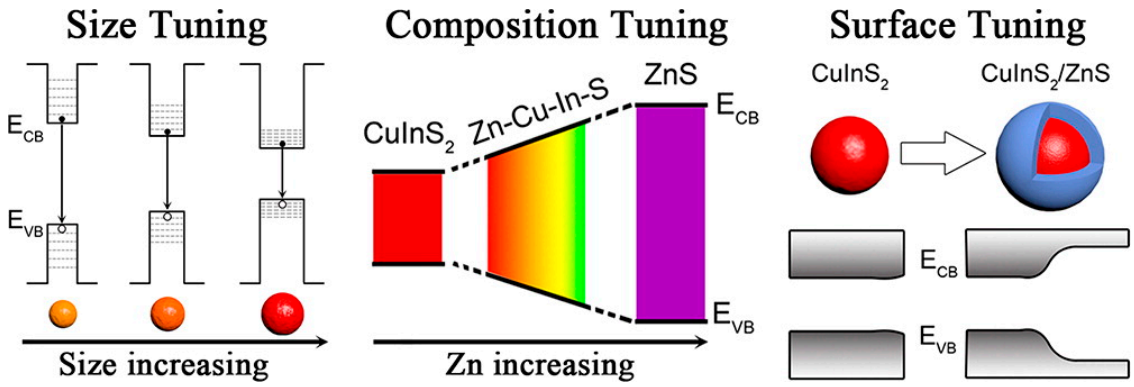

Figure 1. The strategies (size tuning, composition tuning, and surface tuning) that are applied to synthesize the highly luminescent $CuInS_2$ NCs [26].

Biological application (in vivo and in vitro) using QDs has become an attractive alternative over the conventional fluorophores. Higher quantum yield, photoluminescence efficiency, stability and biocompatibility are the desired characteristics for bioimaging application. Studies have shown that incidence of visible light (400–650 nm) for bio-imaging will be absorbed by the collagen, hemoglobin and lipids, thus making tissue imaging impossible in this spectral region. Therefore, a material with a near-infrared (NIR) window (650 to 1350 nm), where light is expected to have maximum penetration depth in tissue and less autofluorescence, is preferred [27]. The preferred intake of quantum dots

by cells is through transfection or receptor-mediated endocytosis rather than through microinjection. Therefore, proper surface conjugation or charge is necessary for their bio application. In addition, before biological application of quantum dots, it is important to tune the surface reactivity, stability, lifetime and biocompatibility of the QDs. This review focuses on the various synthetic strategies (organic and aqueous), formation mechanism, biological applications (in vitro and in vivo) and future perspectives of CuInS-based QDs (Scheme 1).

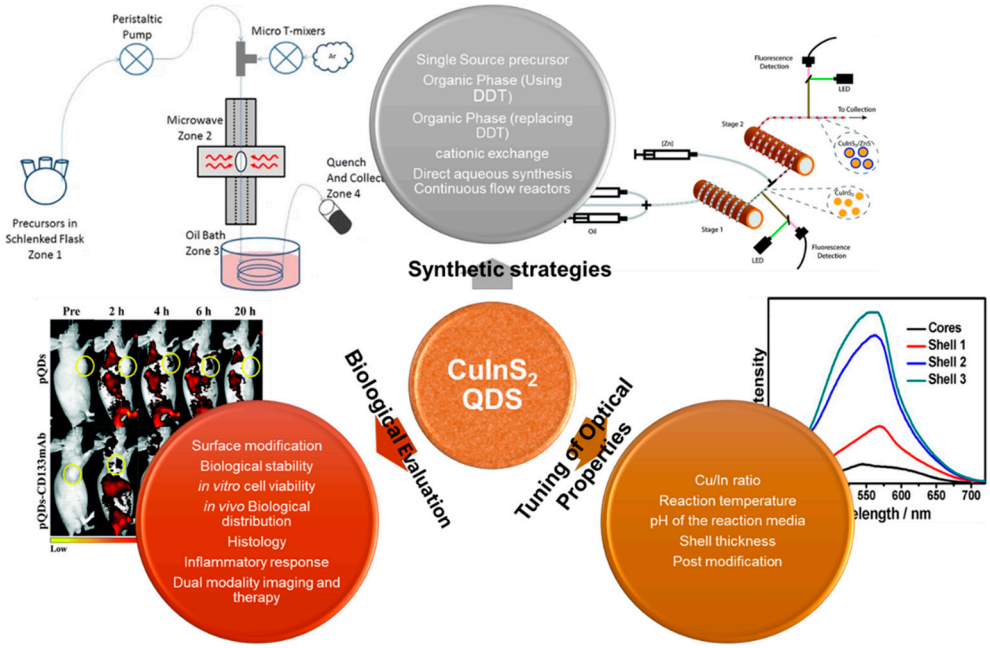

Scheme 1. A schematic representation of the outline of the review.

2. Synthetic Strategies for CIS QDs

The major challenge for the fabrication of CIS QDs is to control the ternary composition. Proper control over composition can lead to the formation of a different crystal structure (cubic to wurtzite structure) [28–31]. Several reports have been published on the synthesis of CIS NCs such as synthesis in solid phase [32,33], hydrothermal (including pressure cooker) [18,34–37], decomposition of single-source precursors [28,38–41] and the hot injection [42–45] method (Table 1). Hirpo et al. [46] reported the conversion of $(Ph_3P)_2$ $CuIn(SEt)_4$ and $(Ph_3P)_2$ $CuIn(SBu)_4$ to CIS NCs. This methodology was vastly used to prepare CIS thin films [47] and colloidal nanoparticles (NPs) [38,48]. From these reports, they concluded that thiol groups have a similar bonding ability to Cu and In and can significantly contribute to the formation of CIS QDs. Even though this method is straightforward, it has some disadvantages such as air sensitivity and expensive precursors. Hence, the search for alternative methods is imperative. QDs with desired properties can be achieved by the varying the composition, ratio of the metal precursors, capping agent/stabilizers, type of stabilizers/capping agent, synthesis temperature, post-synthetic modification and passivation shells [8,18–22,28,32,38,40,44].

Table 1. The main synthetic strategies involved in the production of $CuInS_2$ (CIS)-based quantum dots (QDs).

	Advantages	Disadvantages	Ref
Single source precursor	Straight forward	Air sensitivity Expensive precursor High reaction temperature	[28,38–41]
Organic phase (using dodecanethiol (DDT))	Monodisperse High quantum yield(QY) DDT can act as both a stabilizer and a sulfur source	High reaction temperature (>230 °C) Toxic reagents	[20,21,49–51]

Table 1. The main synthetic strategies involved in the production of $CuInS_2$ (CIS)-based quantum dots (QDs).

	Advantages	Disadvantages	Ref
Organic phase (replacing DDT)	Low reaction temperature (~150 °C) Burst nucleation of the core at lower temperature	Toxic reagents	[8,22,52–54]
Seed mediated cationic exchange	Emission position can be easily tuned to 870 nm	Lower PLQY(<1%) Complex procedure	[17,55]
Direct aqueous synthesis (hydrothermal/reflux)	Low toxic reagents Low reaction temperature (60–150 °C) Water soluble (no further phase transfer required)	Low PLQY (2–5%) Difference in reactivity between Cu^+ and In^{3+} is very high Requirement of dual stabilizer (most cases)	[14–16,56–61]
Continuous flow reactors	Large scale production Minimize the clogging control over the nucleation and growth stage	Expensive	[62–68]

The effect of stabilizing ligand on the structure and properties of CIS NCs was studied by Zhong et al. [21]. A mixture of CuAc, $In(Ac)_3$ and dodecanethiol (DDT) was heated with DDT serving as an ideal stabilizing ligand for the synthesis of CIS NCs and with the help of non-coordinating solvent octadecene (ODE). Liang et al. [49] also used non-coordinating solvent octadecene and dodecanethiol (DDT) in the synthesis of CIS QDs. The DDT acted as both a stabilizing agent and a sulfur source. This resulted in a monodisperse NCs, as shown in Figure 2.

In another development, Zhong et al. [20] used CuI (soft acid and soft base) instead of CuAc and DDT as a sulfur (S) source. In CuAc, Cu^+ is a soft acid and Ac^- is a hard base, while CuI consists of a soft acid and a soft base complex, which will have a good binding ability [50]. In order to reduce the reaction between Cu^+ and the S source (DDT), Zhong et al. introduce oleic acid, which can reduce the reactivity between the thioligand (RSH) and indium ions. This resulted in the formation of a pyramidal shape which was explained by the "surface face polarity model", as shown in Figure 3. The chalcopyrite CIS QDs was obtained from the II-VI zinc blende phase by the substitution of group I (Cu) and group III (In) atoms for group II atoms. Due to the high polarity of the (112) plane in the CIS tetragonal phase, the surface energy increased and grew very fast along the [112] direction. Similar results were observed by Chetty et al. [51].

The above-mentioned protocols resulted in the CIS QDs with a PL emission peak between 550 and 820 nm. For the tunability towards higher wavelength emission, Stam et al. [17] utilized cationic exchange process to synthesize CIS QDs from $Cu_{2-x}S$ seeds. They were able to produce CIS QDs with an emission position at 870 nm, which was difficult to attain through direct synthesis. The crystal structure of the obtained QDs was a hexagonal wurtzite (WZ) structure instead of the cubic chalcopyrite (CP), which is usually observe during the direct synthetic methodology. However, the PLQY was much lower (<1%) when compared to the direct methodology (5–10%). To solve this issue, Xia et al. [55] converted $Cu_{2-x}S$ NCs to WZ CIS QDs by using trioctylphosphine (TOP)/In ratio of 0.9, which balanced the Cu^+-extraction and In^{3+} incorporation. The resultant core CIS QDs was coated with WZ ZnS shells (Zn(St) as Zn source), and this resulted in high PLQY material (75% at 820 nm and 25% at 1050 nm).

The major drawback in this method is that it involves high temperature due to the high decomposition temperature of DDT and its complex procedure.

In another study, Nose et al. [52] used amine surfactants hexadecylamine (HDA) and oleylamine (OLA), which can effectively stabilize the CIS QDs, as a replacement for DDT. Pan et al. [8] used the hot injection method with $CuCl_2$, $InCl_3$ and NaS_2CNEt_2 as precursors and obtained zinc blende and wurtzite CIS. They were able to tune the particle size by altering the temperature and capping agent (OLA). Han et al. [53] used a solvothermal method to synthesize CIS chalcopyrite structure by initially forming a Cu^{2+}–thiourea complex which reduced the Cu^{2+} followed by the crystallization of Cu^{+}, S^{2-} and In^{3+} in the presence of octadecylamine. Yu et al. [54] also followed a similar approach by using 4-Bromo thiophenol (HSPh) as a thioligand and observed a color change during the addition of the ligand to the metal precursors. This color change (disappearance of blue) was attributed to the reduction of Cu (II) to Cu (I). The growth of $CuInS_2$ QDs involved solvothermal decomposition of a soluble molecular intermediate $NaCuInS(SPh)_m$ formed by mixing the chemicals (e.g., $CuCl_2$, $InCl_3$, HSPh and Na_2S) at room temperature. To solve the requirement of high injection temperature and to generate burst nucleation, Li et al. [22] used Na_2S as a sulfur source with 50 times the stoichiometric ratio of CIS and OA as a capping agent. This excess sulfur source increased the reaction of the precursors ($CuCl_2$ and $InCl_3$) with sulfur, shortened the nucleation stage and lowered the temperature (150 °C). The lowering of the temperature did not affect the monodispersity and crystallinity of the material, as shown in Figure 4.

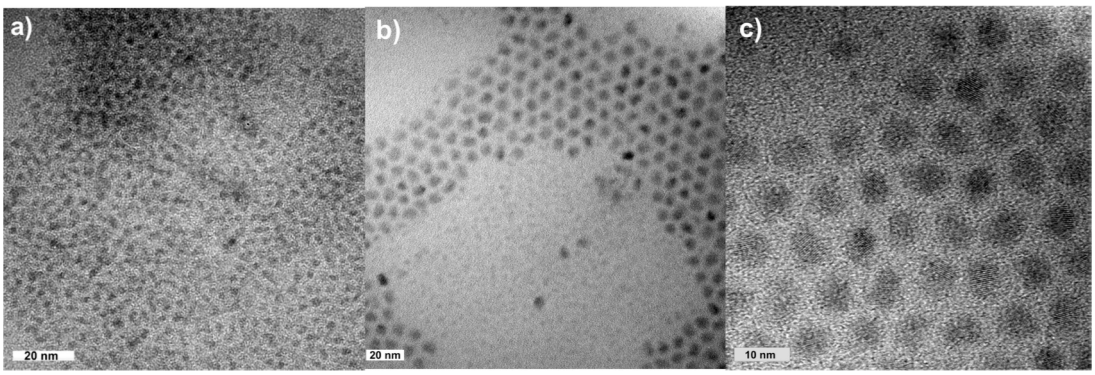

Figure 2. TEM images of (**a**) CIS QDs and (**b**,**c**) the corresponding CIS/ZnS QDs with different magnifications (synthesized using DDT as a capping ligand) [69].

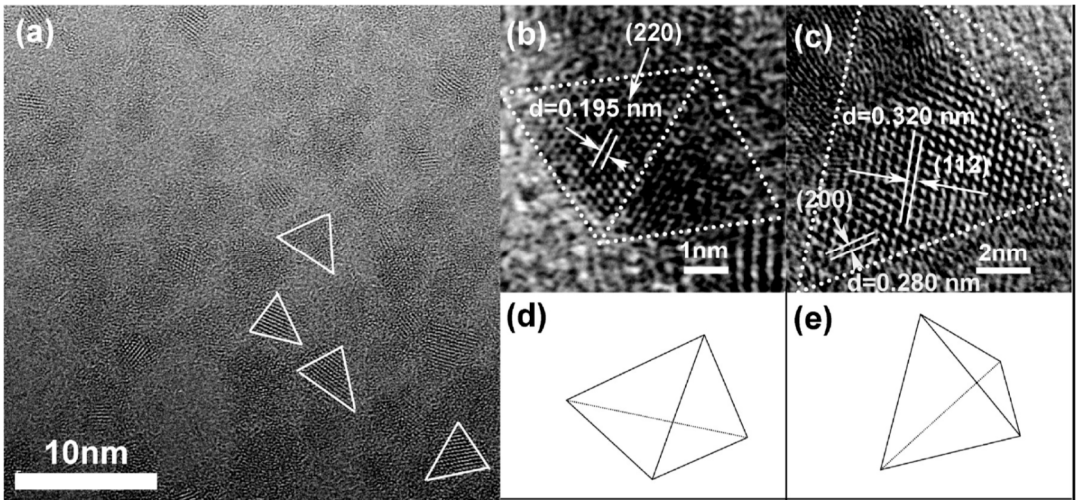

Figure 3. (**a**) High Resolution Transmission Electron Microscope (HRTEM) images of CIS QDs; (**b**,**c**) HRTEM images of a single CIS QDs; (**d**,**e**) schematic diagrams of CIS pyramids in (**b**,**c**), respectively [20].

The CIS QDs' long-term stability was an important issue for further application. Therefore, the researchers were focusing on the production of a type I core/shell structure (e.g., CIS/ZnS) to enhance the PL stability and QY. In the beginning, zinc ethyl xanthate and zinc diethyl dithiocarbamate were used as the Zn source. Later, Park et al. [70] used zinc acetate as zinc precursors at 210 °C under N_2 atmosphere. The study was extended towards different zinc precursors such as zinc chloride, zinc stearate and zinc acetyl acetate, and the researchers observed a huge blue shift (irrespective of the Zn source) (Figure 5) in the emission position, which was attributed to cation diffusion into the core at high temperature.

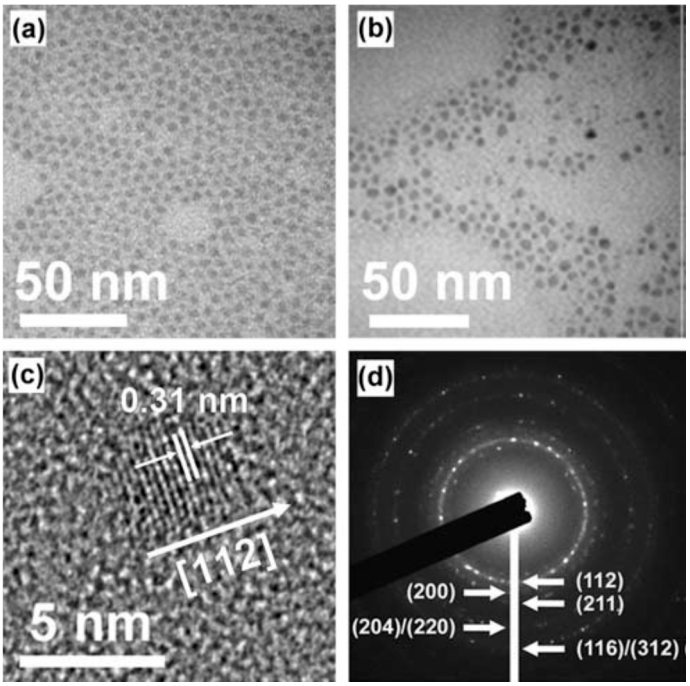

Figure 4. TEM images of the $CuInS_2$ QDs grown with excess Na_2S for 1 h at (**a**) 150 °C and (**b**) 170 °C. (**c**) HRTEM image of the as-prepared $CuInS_2$ QDs grown at 150 °C for 1 h with visible lattice fringes. (**d**) Selected-area electron diffraction pattern of the 150 °C $CuInS_2$ QDs. The arrows point to where the vertical white line crosses the crystal face rings. [22].

The above methods involved expensive, toxic, unstable and hazardous precursors/solvents. Thus, water-soluble CIS QDs were preferred. Some researchers have tried to obtain water-soluble CIS QDs through the ligand exchange process [55,56,69,71–73]. This ligand exchange method is very complicated, and it also affects the PLQY after aqueous transfer [72]. Therefore, direct synthesis of CIS QDs is preferred. From the previous results, hydrophobic solvents such as 1-dodecanethiol, OLA etc. were used to control the reactivity of cations (Cu and In) [74–76]. However, in aqueous solution, the difference in reactivity between Cu^{+} and In^{3+} is very high. As discussed earlier, Cu^{+} is a soft acid and In^{3+} is a hard acid. Therefore, soft bases such as water-soluble L-glutathione (GSH), thiomalic acid, 3-mercaptopropionic acid, L-cysteine and thioglycerol are usually used as capping agents. Liu et al. [77] designed a direct strategy for the synthesis of CIS QDs in water using MPA (mercaptopropionic acid) as a stabilizer via the hydrothermal method. Despite this, in the previous methods involving organic methods, the temperature was varied between 160 to 300 °C. In this method, the best results were obtained at 150 °C. However, these ligands had low complex stability towards In^{3+} (hard acid), which caused phase separation. To solve this issue, a secondary ligand-containing a multicarboxylate group (e.g., sodium citrate) was proposed to control the reactivity of the In^{3+}. Chen et al. [14] synthesized water-soluble CIS QDs using a dual capping agent (GSH) and sodium citrate (temperature: 95 °C). For the core synthesis, high-reactive Na_2S was used as a sulfur source, while for the shell, low reactive thiourea was used. One disadvantage of this method is the use of low temperature in the presence of a high-reactive Na_2S source, as this resulted in rapid nucleation of the core. This rapid nucleation at low temperatures can introduce large defects in the CIS core, which subsequently lower the QY. However, as reported earlier, a type I shell (e.g., ZnS) can solve this issue by effectively passivating the core. Blue shifting of the emission peak was also seen in this low temperature aqueous synthesis, confirming the diffusion of zinc ions even at low temperature, as shown [56,57] in Figure 6. This method was supported and modified by Jia et al. [58], Mir et al. [15] and Tsolekile et al. [59]. By following these methods, Xie et al. [60] reported a one-pot synthetic strategy using ribonuclease A (RNase A) as a stabilizer and CuI, $InAC_3$ and thiourea as metal and sulfur precursors. Even though the above methodologies are facile for aqueous synthesis of CIS/ZnS core/shell QDs, low QY (2–5%) without ZnS passivation is a problem [14,61]. To solve this issue, Arshad et al. [16] introduced a green strategy by using a low temperature (100 °C) and a longer reaction time (8 h) in an autoclave to produce CIS QDs with 14% QY. During the one-pot aqueous synthesis of CIS QDs, the usage of short-chain thiols was said to be undesirable because they hydrolyze/pyrolyze partially, and the rate of sulfur release was very low at high temperature.

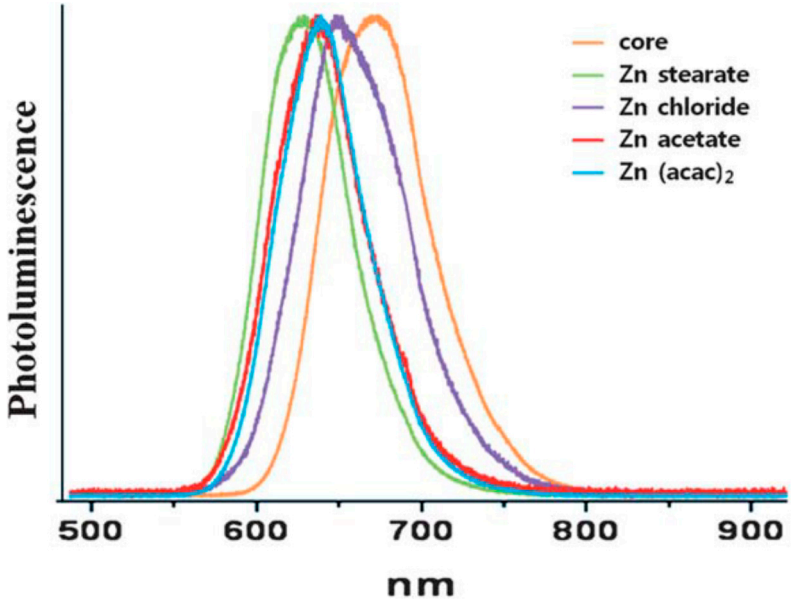

Figure 5. Blue-shifted emission spectra with different Zn precursors [70].

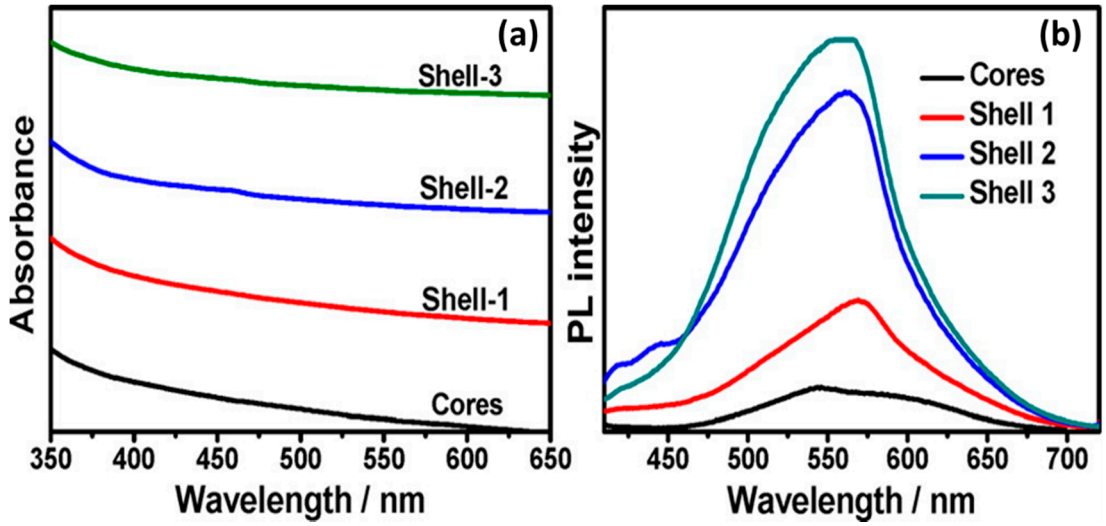

Figure 6. UV-vis absorption (**a**) and PL (**b**) spectra of Cu−In−S core QDs and Cu−In−S/ZnS core/shell QDs with deposition of different thicknesses of the ZnS shell around the core QDs that were synthesized in water [14].

To solve this issue, Zhang et al. [78,79] used H_2S gas as an in situ sulfur source for the CIS core and thioglycerol (TG) as a sulfur source for the ZnS shell. However, the control over the generation of H_2S was difficult, thus, the presence of ligands was crucial for the synthesis of CIS and CIS/ZnS QDs. The ligand should stabilize the QDs, act as a sulfur source and balance the reactivity of the metal precursors.

For the industrial application of the CIS-based QDs, large scale synthesis is very important. The conventional hot injection method [80] gives total control over the QDs' size distribution. However, this method involves the injection of reactants into the high-temperature environment, which will only be effective for smaller volumes where the secondary reagents can be added and mixed quickly [81]. For the non-injection or heat method, the synthetic protocol involves the mixing of precursors and reagents into one pot and heating for the nucleation process [82,83]. This protocol suffers lack of temperature uniformity between walls and solution, which affects the uniform nucleation and growth.

To solve these issues, a new setup known as the continuous flow reactor (CFR), in which the reagents were pumped through the heating zones, was proposed [62,63]. However, this method also led to problems, such as clogging of the reactor and poor material quality. Then, the microwave-assisted continuous flow reactors (MWCFR) were introduced, which can minimize the clogging, as shown in Figure 7. Fitzmorris et al. [64] reported the MWCFR method for the production of CIS QDs. The main advantage of this method is the easy tunability of the synthetic parameters and distinct control over the nucleation and growth stage. The QDs undergo a cation exchange process with zinc followed by the growth of the shell. The final core/shell QDs is reported to exhibit the desired composition, with a PLQY of 65%.

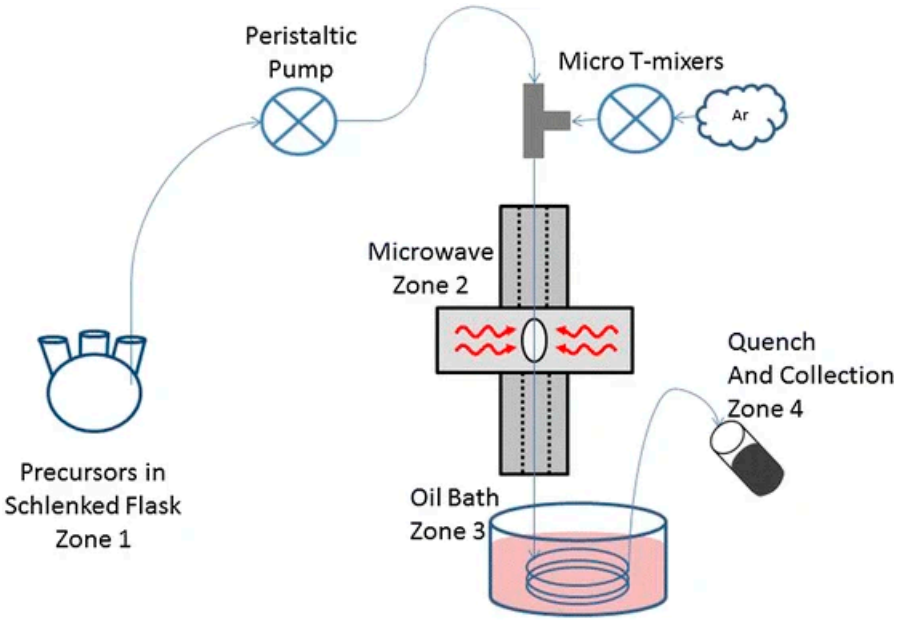

Figure 7. MWCFR used for the synthesis of CIS QDs. Precursor solutions are prepared in an air-free three-necked flask on a Schlenk line, and peristaltic pumps are used to move the solution through polytetrafluoroethylene (PTFE) tubing into the microwave heating zone, through an oil heating bath, and finally into the sealed collection vial under N_2 gas [64].

A large mass and heat transfer with the microfluidic environments, good decoupling of nucleation, growth strategies and fast parametric screening of reaction parameters for fast optimization are the advantages of microfluidic reactors [84–86]. Continuous microfluidic synthesis of core/shell NCs was also reported [65,66]. However, the effective continuous flow of microfluidic reactors for the generation of core/shell QDs with desired composition and size was affected by the microfluidic channel [84,85]. To solve this issue, multistage synthesis via a droplet-based protocol was proposed [67]. Yashin et al. [68] reported controlled synthesis of CIS/ZnS NCs through a two-stage droplet-based microfluidic platform, as shown in Figure 8. The advantage of this system was the control over the reaction parameters, such as temperature, time and composition, which resulted in high-quality photostable CIS/ZnS QDs. In addition, the setup did not need a prior purification of the core before shell growth.

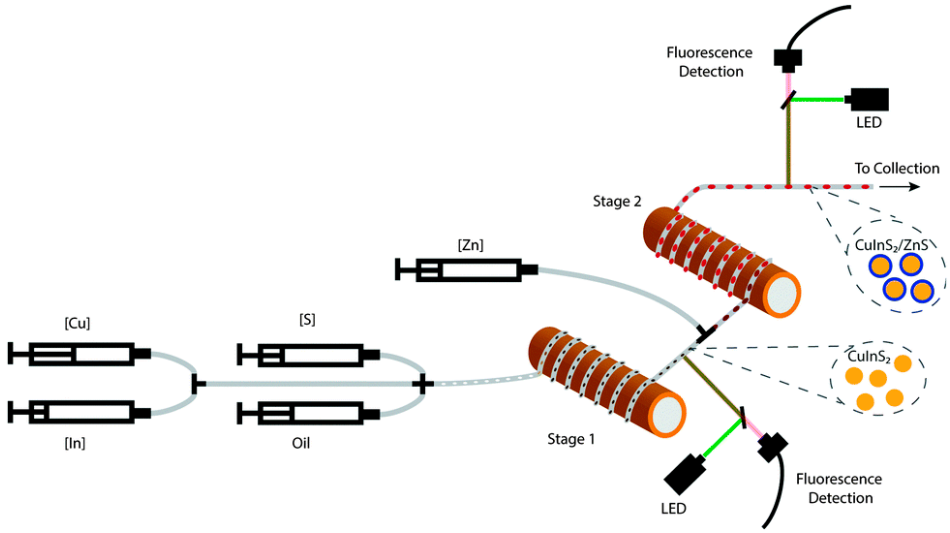

Figure 8. Two-stage droplet-based microfluidic platform for the controlled synthesis of $CuInS_2/ZnS$ NCs [68].

3. Tuning of Optical Properties of CIS QDs

To improve the PL emission of the CIS QDs, the most common strategies employed are the coating of shells and alloying strategies [13–15,18,42,43,55,56,58,59,61,65,66,68–70,72,74,75,78,87–90]. Earlier studies revealed that stoichiometry control is important in obtaining highly luminescent CIS QDs [20,21]. From the theoretical and experimental studies, the intrinsic defects in CIS QDs were found to be dependent on off stoichiometry. Maeda et al. [91] reported an off stoichiometric effect on the PL emission of CIS QDs synthesized through the hot injection method. The tuning of the Cu/In ratio greatly enhanced the PL properties. By following this method, Chen et al. [92] controlled the composition of CIS NCs by varying the molar ratio of CuI and $In(OAc)_3$. When the Cu/In ratio was between 1.3 to 0.3, all the samples emitted in the red region (650–700nm). However, there was a blue shift in the emission position with constant FWHM (120 nm) when the Cu/In ratio was reduced. A maximum QY of 11% was achieved at a Cu/In ratio of 0.7. These results showed that good luminescent CIS particles can be obtained in Cu-deficient samples and suggested a donor–acceptor pair recombination mechanism (DAP), in which the PLQY of the CIS can be tuned with defect concentrations, as shown in Figure 9.

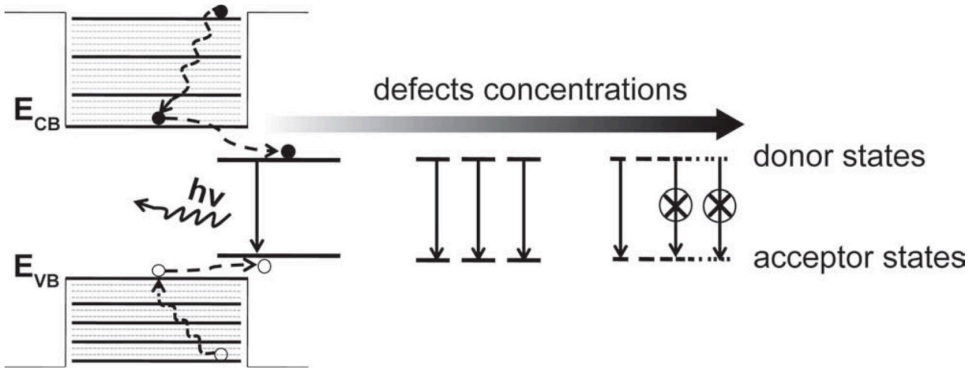

Figure 9. A schematic diagram used to demonstrate the photoluminescence (PL) properties of $CuInS_2$ NCs [92].

Different antisites (In_{Cu}, Cu_{In}), interstitial sites (Cu_i, In_i) or vacancies (V_{Cu}, V_{In}, V_S) are the defects which influence the optical properties. With chalcopyrite CIS materials, it is easy to introduce crystal defects because of the weak Cu–S bond [93–95]. Uehara et al. [91] introduced copper vacancy and indium substitute to tune the optical properties of the CIS QDs (in the presence of oleyl amine and

DDT). The Cu/In ratio was tuned from 1:1 to 1:7. The PL emission increased as the Cu/In ratio decreased. There was also a blue shift in the PL emission (730–690 nm) when the Cu/In ratio was decreased. This shift was explained with the widening of the band gap.

Klimov et al. [96] explained the key role of copper deficiency as intergap emission centers for CIS QDs. Jawahar et al. [4] also studied the dependence of the Cu/In ratio (0.7:100, 3:100, 6:100, 12:100, 18:100). By increasing the Cu content, there was a red shift in absorption spectra and absorption edge wavelength. Moreover, there was a red shift in the emission peaks from 594 to 616 nm. The PLQY was at its maximum (~18%) at the Cu/In ratio of 12:100. They also varied the reaction temperature from 60 to 100 °C and observed a temperature-dependent PL emission. There was an increase in PLQY and red shifting of the emission position as the temperature of the reflux increased from 60 to 100 °C. This change was attributed to the reduction in the band gap energy. The most significant enhancement in the optical properties in the aqueous method was reported by Pan et al. [14] and Zhang et al. [97]. Zhang et al. [79] investigated the dependence of the Cu/In ratio (1:1, 1:2, 1:4) on the optical properties of CIS and CIS/ZnS QDs synthesized via an aqueous method (MPA, Dimethylformamide(DMF) and H_2S as the S source). A blue shift in the absorption band was observed as Cu content was reduced due to the increase in the band gap [98]. A reduction in the Cu content resulted in a weak repulsion between d orbitals of copper and p orbitals of sulfur. This lowered the valence band and thus increased the band gap [90]. There was also a blue shift in PL emission as Cu content was reduced. Recently, our group studied the effect of the Cu/In ratio (1:1, 1:8, 1:12), pH and the amount of capping agent on the optical properties of CIS QDs synthesized via the direct aqueous method [99]. At 1:1, the emission intensity was very low; however, at 1:4, the emission intensity was at its maximum at a position of 730 nm. When the ratio was further increased (1:8 and 1:12), there was a blue shift in the emission position with reduced PL intensity. The QDs synthesized at lower pH (~3.6) exhibited high PL emission. When the pH of the solution was moved to the alkaline condition, the PL emission was blue shifted with a decrease in PL intensity. This pH-dependent emission spectra were explained with respect to the high bonding affinity of the capping ligand(GSH) towards the metal precursor at low pH.

The Cu/In ratio did not only affect the PLQY, but it also affected the photostability. Increasing the shell thickness was one of the methods proposed by Ma et al. [100]. These thick shells are expected to eliminate the defects and increase PL stability. The thick shell effectively isolated the core CIS from photoinduced corrosion (Figure 10). Recently, our group reported a green procedure for the synthesis of CIS QDs followed by post-modification using different concentrations of sodium alginate (SA) biopolymer at different temperatures [2]. The alginate-passivated CIS QDs showed a 36% increase in photostability and 2-fold increase in QY at a ratio of 1:8 (SA/CIS). The results suggested that, during photoirradiation, the existing and photoinduced surface traps of the charge carriers could be immediately eliminated by hydroxyl and carboxyl groups of SA.

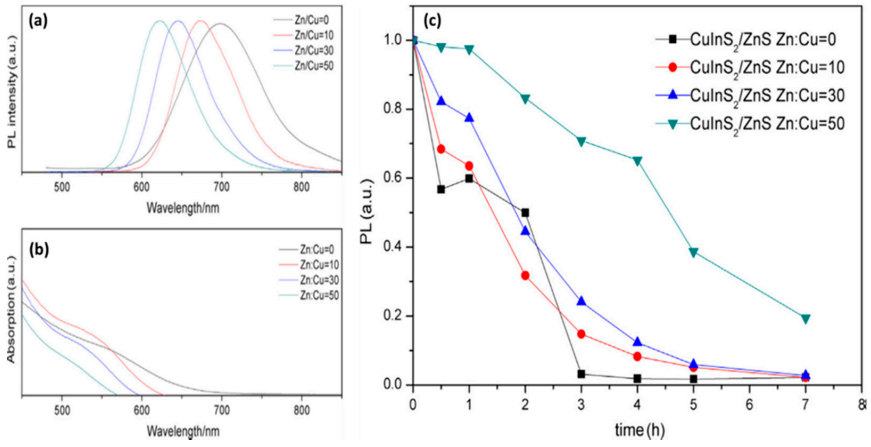

Figure 10. PL: (**a**) UV-vis spectra (**b**) and photostability spectra (**c**) of CIS and CIS/ZnS with different Zn ratios [100].

4. Biological Evaluation of CIS-Based QDs

There are very few reports on the in vivo stability and toxicity studies on CIS-core QDs without shell or surface conjugation. The first in vivo evaluation of CIS-based QDs was reported by Li et al. [49]. The materials were injected into the tail of mice and were evaluated using fluorescence reflectance imaging (FRI). After 15 min of injection, the QDs were seen accumulating in the liver, spleen and lungs. After 24 h, dissection was performed, and the materials were reported to be noninvasive (Figure 11). This showed the potential application of CIS/ZnS for imaging.

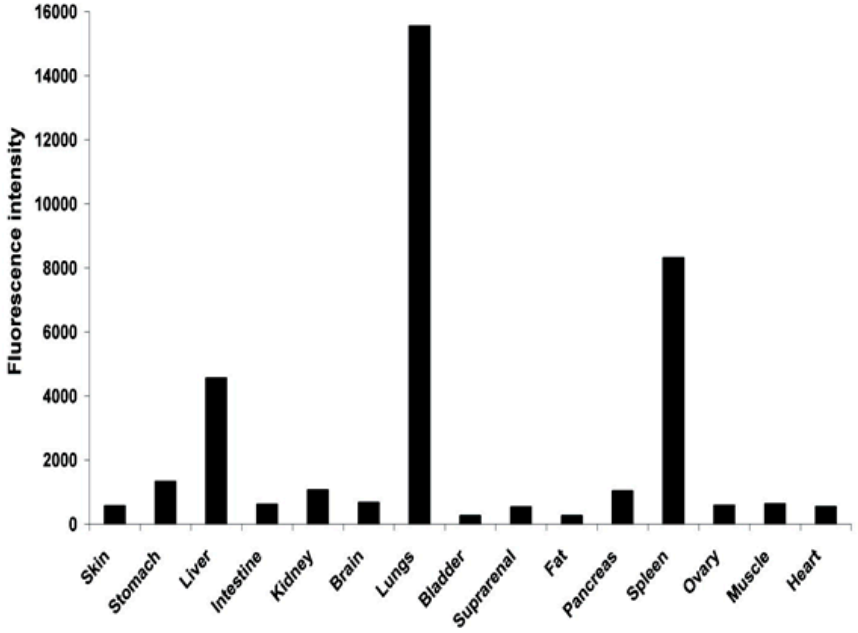

Figure 11. Biodistribution of the CIS/ZnS NCs 24 h after tail vein administration of a mouse [49].

In another report, Kays et al. [10] used the murine model to study the in vivo biodistribution and cytotoxicity of $CuInS_2$ (CIS), Zn-doped $CuInS_2$ (CISZ) and $CuInS_2$/ZnS QDs on different days (1, 7 and 28 days). They observed a quick clearance, and less than 25% of the material was found in the organs after 28 days. They also studied the in vivo toxicity of the QDs by recording organ indexes (Figure 12). The organ index can be explained as the organ weight divided by the total body weight. For CIS and CISZ, there was a significant increase in liver and spleen organ index, but there were no significant changes observed for CIS/ZnS QDs. The kidney size variation was inconsistent, and only CIS and CIS/ZnS showed a significant change.

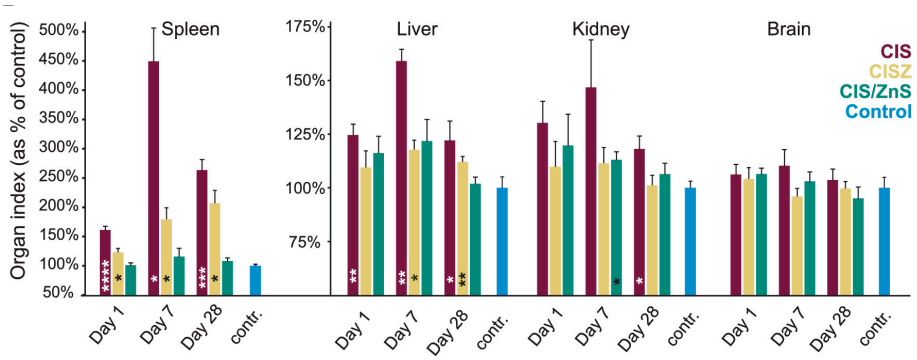

Figure 12. Organ index (organ weight/total body weight) plotted as the percent of control values for four major organs [101].

To further confirm the organ specific toxicity, they studied the histopathology of the mouse (Figure 13). For the liver, they observed geographic necrosis with the CIS QDs. For the CISZ, there was only small inflammation. In case of the spleen, CIS- and CISZ-treated cells exhibited multinucleation, which was the result of inflammatory response. In addition, disruption of spleen architecture was observed with CIS QDs. However, no significant toxicity to the kidney was observed for all the materials. From the results, they confirmed that with the ZnS coating, they were able to minimize the degradation and subsequent toxicity of the material.

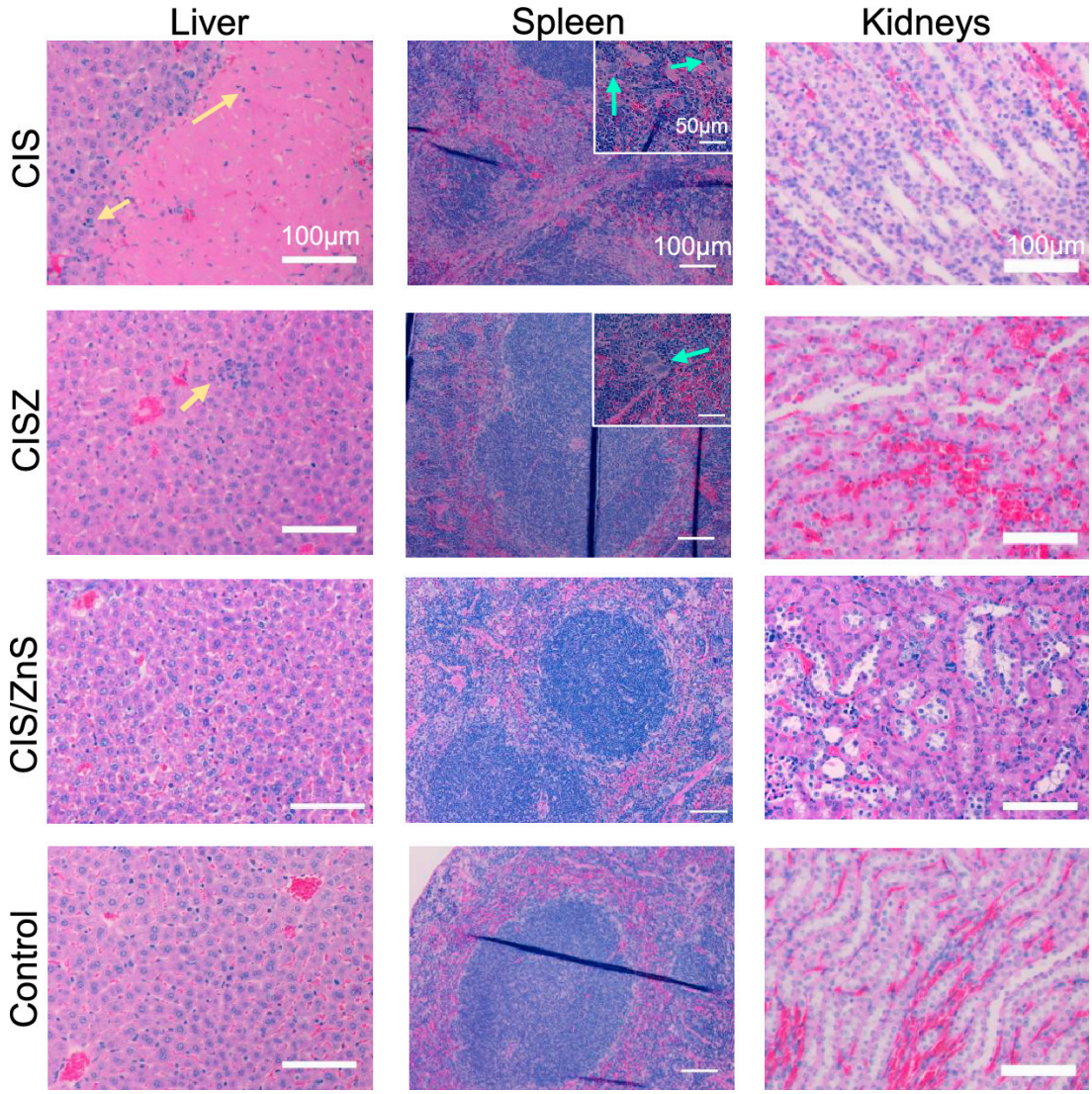

Figure 13. Histology of QD-dosed mice. Left, middle, and right columns show the liver, spleen, and kidney, respectively. Yellow arrows indicate inflammatory cells; blue arrows point to multinucleated giant cells. The scale bar is 100 μm for primary photos and 50 μm for inserts [101].

Pons et al. [102] synthesized CIS/ZnS QDs coated with dipalmitoyl phosphatidyl ethanolamine polyethylene glycol (DPPE-PEG 2000). After capping with PEG, the PLQY was slightly decreased. This material was further evaluated for lymph node compatibility, and the result was compared with PEG-capped CdTe/ZnS QDs. After the injection of both materials in a dose-dependent manner (0 to 100 pmol), the materials showed an inflammatory response to the dosage (Figure 14). However, the inflammatory response was larger for the Cd-based QDs compared to CIS/ZnS QDs due to the acute toxicity of Cd^{2+}. These results suggested that even though the materials were capped with a PEG derivative, some of the inorganic materials were also released during the incubation. Sun et al. [5]

coated CIS/ZnS QDs with a PEG derivative followed by their conjugation to the Ki-67 protein for breast cancer (MDA-MB 2311) therapy. From the fluorescence images, they observed that QDs concentrated inside the nucleus rather than the cytoplasm, and this was attributed to the nuclear-targeting property of the Ki-67 protein.

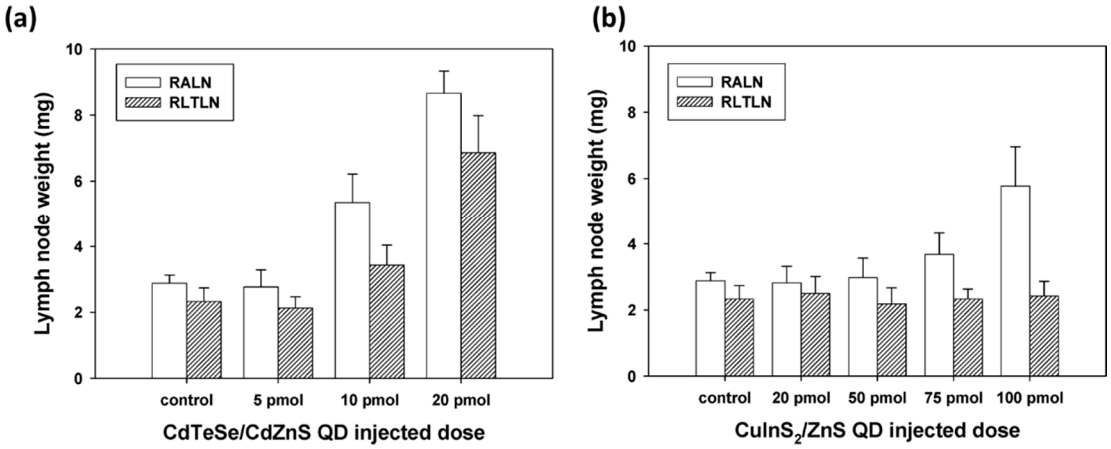

Figure 14. Weight of the right axillary LN (RALN) and right lateral thoracic LN (RLTLN) dissected 7 days post-injection as a function of the QD-injected dose for CdTeSe/CdZnS (**a**) and $CuInS_2$/ZnS (**b**) QDs. The data are mean ± SEM (n = 6 per group) [102].

In another study, Xi et al. [60] introduced a one-step synthetic strategy using ribonuclease A (RNA-ase A) as a stabilizer to improve the water solubility and biocompatibility of the CIS QDs. This material showed good compatibility towards the MC3T3-R cell lines even at 5 mg/mL concentration. Chitosan is a natural biopolymer used by many researchers for drug delivery applications due to its excellent biocompatibility and degradability [103,104]. Deng et al. [105] modified CIS/ZnS QDs with folate-modified N-succinyl-N′-octyl/chitosan and applied this material for in vitro and in vivo imaging. The PL intensity was decreased to 40% after the encapsulation inside the chitosan with no change in average particle size. Both in vitro and in vivo imaging were successful, with excellent biocompatibility. In continuation with this report, Chen et al. [106] investigated the toxicity of chitosan-capped CIS and CIS/ZnS QDs. The modification with the chitosan decreased the emission intensity to 60% with an increase in particle size from 2.3 nm to 100 nm. The cytotoxicity towards Hela and Human Oral Squamous Carcinoma Cell Lines (OECM 1) were evaluated. From the results, the chitosan-coated CIS and CIS/ZnS QDs showed excellent biocompatibility, even at 250 µg/mL (Figure 15). The confocal microscopy showed that the QDs were effectively taken inside the cells. The chitosan modification was further confirmed and studied by Kim et al. [69].

These capping of CIS-based QDs with amphiphilic and other agents improved the biocompatibility and solubility of the material. However, the stability of these QDs in high ionic strength media like biological fluid is a concern. Silica shells are usually used for binary QDs due to their non-toxicity, chemical stability and optical transparency [107]. Hsu et al. [108] encapsulated CIS/ZnS QDs inside the silica matrix and observed an improvement in cell viability and stability. Foda et al. [109] synthesized CIS/ZnS QDs and encapsulated them inside lipophilic silane. The silica coating did not affect the emission intensity compared to other coating strategies. The stability of the silica QD hybrid was evaluated in H_2O, phosphate buffer (PBS) and Dulbecco's Modified Eagle Medium (DMEM), and the result showed excellent stability (Figure 16) and biocompatibility. The improvement in colloidal stability was attributed to the stable crosslinked silica layer around the QDs, which effectively protects the QDs from aggregation.

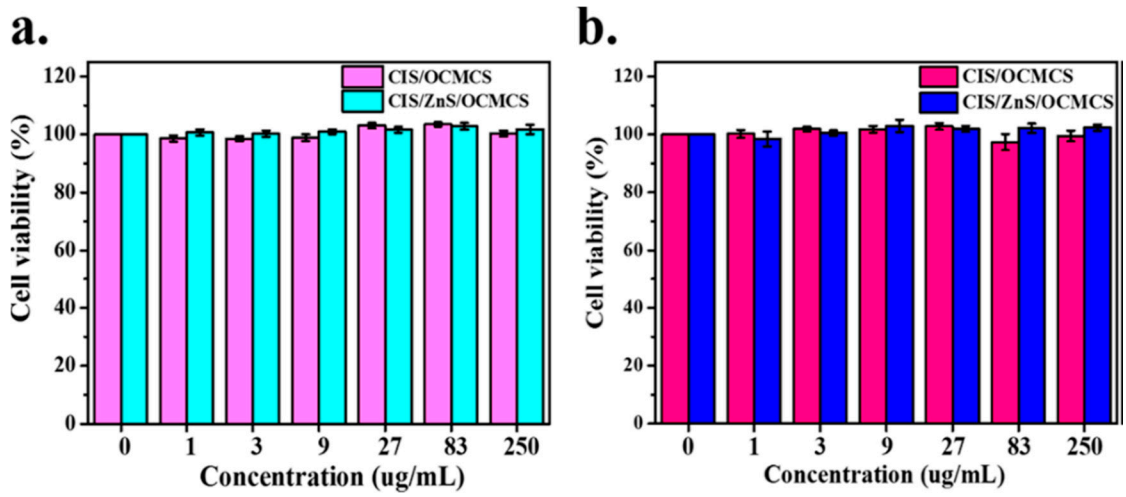

Figure 15. In vitro cell viability test of (**a**) Hela and (**b**) Human Oral Squamous Carcinoma Cell Line (OECM) incubated with different concentrations (1, 3, 9, 27, 83, and 250 μg/mL) of CIS/OCMCS (O-carboxymethylchitosan coated $CuInS_2$ QDs) and CIS/ZnS/OCMCS QDs in cell medium for 72 h [106].

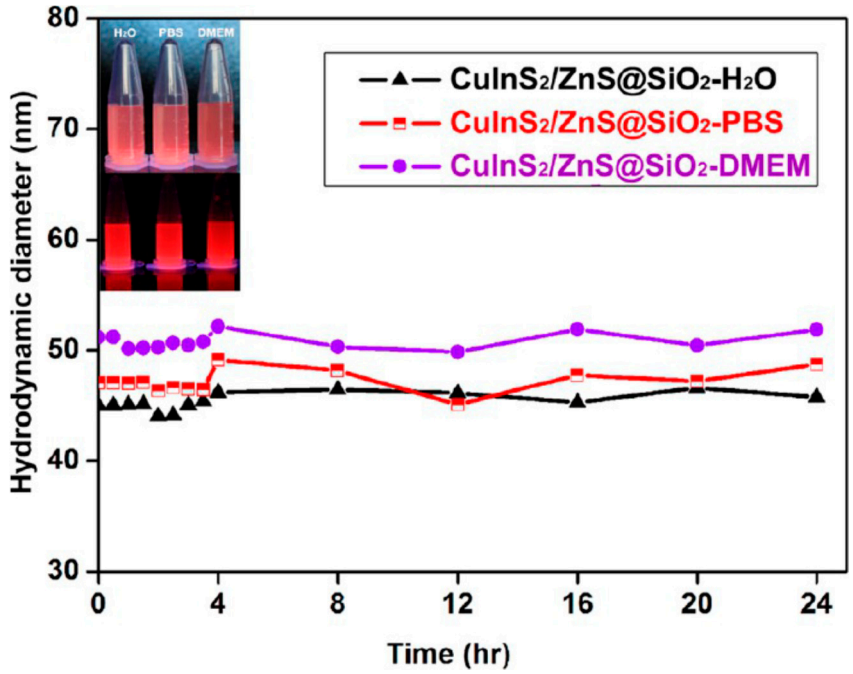

Figure 16. Hydrodynamic diameters of $CuInS_2$/ZnS@SiO_2 nanoparticles in Deionised water, PBS, and DMEM incubated at 37 °C. Inset: digital photographs of $CuInS_2$/ZnS@SiO_2 in different media under room light (upper) and UV light (lower) [109].

Mesoporous silica nanostructures (MSNs) have been reported to be successful carriers for drug delivery [110], and rod-shaped MSNs (e.g., Santa Barbara Amorphous (SBA15)) have shown superiorities in biomedical applications. Recently, our group reported the synthesis of $CuInS_2$/ZnS (CIS/ZnS) quantum dots (QDs) followed by sodium alginate (SA) postmodification and loading into the mesoporous channels of SBA15 (Figure 17) [3]. There was a red shift in emission position of the QDs after the encapsulation with an increase in intensity. Furthermore, the photostability of the QDs was greatly enhanced by the modification. Furthermore, the material exhibited excellent biocompatibility towards A549 and HEK 293 cancer cell lines, which paved the way for rational designing of ternary QDs for biological applications.

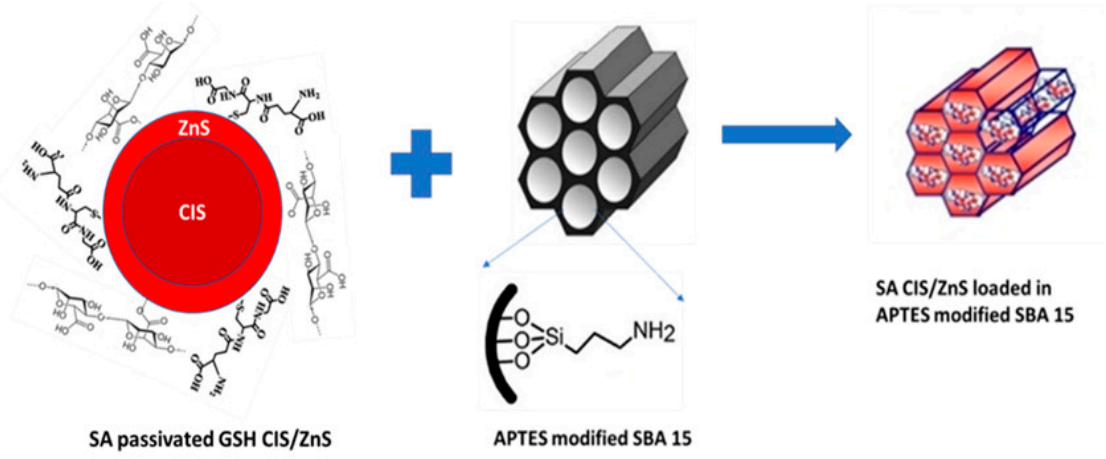

Figure 17. Schematic representation of the encapsulation of sodium alginate passivated CIS/ZnS QDs in amine-modified mesoporous silica [3].

Though CIS QDs have been useful successfully for imaging application, there is still a concern on deep tissue imaging and targeting using only CIS QDs. One way of solving this problem is by dual imaging. Dual modality imaging using magnetic resonance (MR)/fluorescence has a lot of advantages [111,112]. MR imaging has been reported to have high resolution and deep penetration [113,114]. Shen et al. [115] loaded Fe_3O_4 and CIS QDs in a silica shell followed by functionalization with arginylglycylaspartic acid (RGD) for targeted therapy. The emission was reduced and red-shifted after encapsulation and functionalization, which might be due to the change in surface charge. The silica hybrid particle showed excellent biocompatibility towards BXPC-3 cells, even at 2 mg/mL concentration. The in vivo MR imaging showed a clear enhancement of T1-weighted positive and T2-weighted negative. In another study, Zhang et al. [116] conjugated CIS/ZnS QDs with Gd^{3+}-functionalized Bovine serum albumin (BSA) protein followed by conjugation with the anti-CD133 antibody for tumor-targeted bimodal imaging. The PL emission intensity of the CIS/ZnS QDs was not affected by the surface modification, but a slight redshift was observed. The functionalized QDs were evaluated in a glioma tumor model. The results (Figure 18) showed that antibody-linked QDs displayed excellent fluorescence compared to that which was not functionalized. Initially, they observed a large accumulation of NPs in the liver, but over time, this started to decrease due to the metabolism of the particles. Even for MR T1-weighted evaluation, the antibody-conjugated QDs showed a higher contrast signal. This shows that the functionalization of CIS QDs with targeting ligands can improve the biological application.

Recently, our group reported the conjugation of meso-tetra-(4-sulfonatophenyl) porphyrin (TPPS4) and meso (hydroxyphenyl) porphyrin to the CIS/ZnS QD conjugate in order to improve the singlet oxygen generation of the porphyrin for multimodal imaging and therapy [18,117]. The cytotoxicity of CIS/ZnS and the TPPS4-CIS/ZnS conjugate was evaluated on a normal cell line (BHK 21) and a cancer cell line (THP-1). Both CIS/ZnS and the conjugate showed excellent biocompatibility towards the normal cell line, but for the cancer cell line, the results were dose dependent with more cytotoxicity observed for the CIS/ZnS-TPPS4 conjugate (Figure 19). The singlet oxygen evaluation of the as-synthesized porphyrin and conjugate was measured using 1,3-diphenylbenzofuran (DPBP) as an oxygen scavenger under irradiation of 657 nm laser light. After the conjugation of porphyrin to QDs, the singlet oxygen quantum yield (SOQY) increased from 0.27 to 0.72. This increase was attributed to the fluorescence resonance energy transfer (FRET) between be the QDs and the porphyrin.

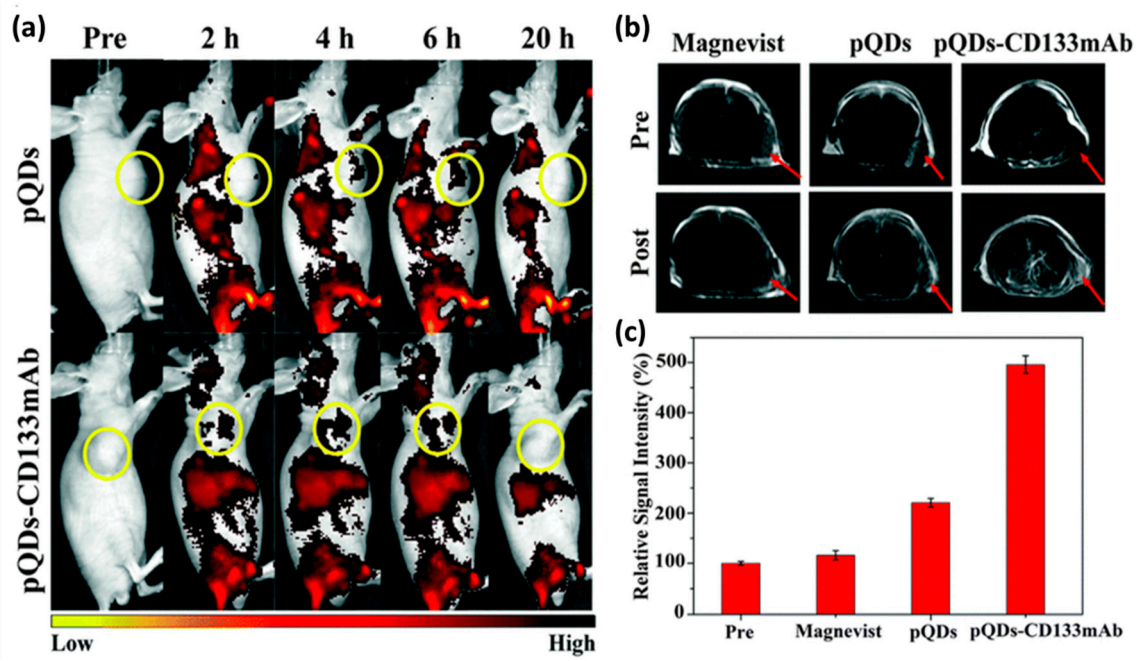

Figure 18. (**a**) In vivo fluorescence images of nude mice-bearing CD133+ glioma tumors indicated by the yellow circles before and after intravenous injection with hydrophilic paramagnetic QDs (pQDs) and CD133mAb-pQDs. The excited wavelength was 470 nm. (**b**) In vivo T1-weighted magnetic resonance (MR) images of nude mice-bearing CD133+ glioma tumors before and after injection of pQDs-CD133mAb, pQDs and Magnevist (4 h). (**c**) Relative T1 enhancement values of the glioma areas before and after injection of Magnevist, pQDs and pQDs-CD133mAb, respectively [116].

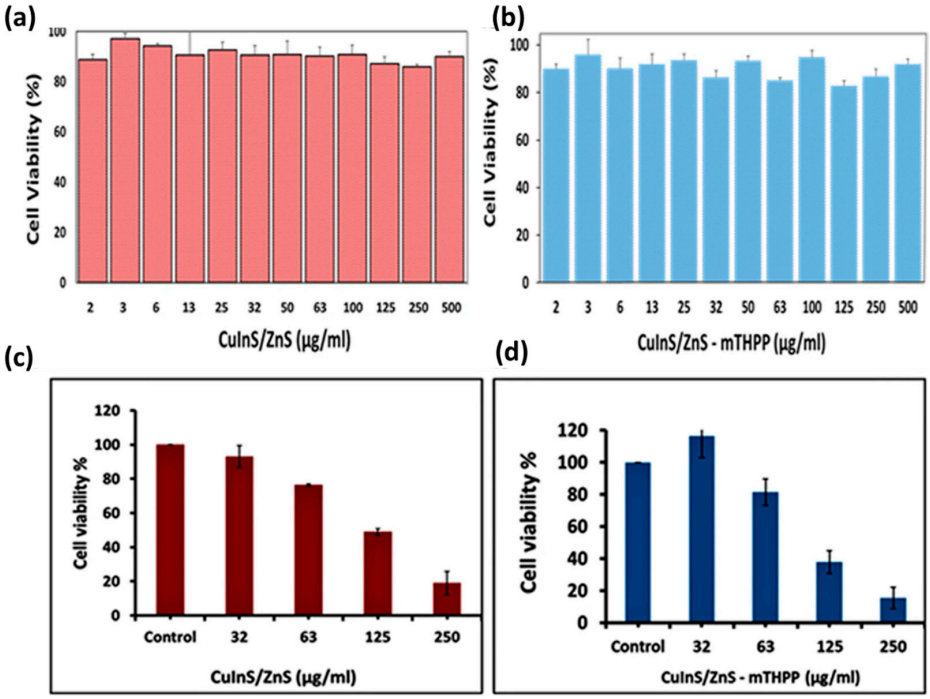

Figure 19. Cell viability study of (**a**) $CuInS_2$/ZnS QDs and (**b**) $CuInS_2$/ZnS-mTHPP(meso (hydroxyphenyl) porphyrin) conjugate QDs against BHK21 normal cell line and Cytotoxicity studies of (**c**) CuInS/ZnS QDs and (**d**) CuInS/ZnS—mTHPP conjugate against THP-1 cancer cell line [18].

5. Conclusions and Future Outlook

$CuInS_2$ (CIS) has been reported as an alternative to Pb-, As-, Cd- and Hg-based QDs due to its toxic free composition. Moreover, its PL can be easily tuned towards NIR regions by varying its composition. The CIS/ZnS QDs synthesized through organic method have excellent PLQY, but their effective application is hindered due to the hydrophobic nature and toxicity of the reagents used. However, the hydrophobic QDs can effectively be transferred into aqueous media through the ligand exchange process, which can facilitate their use in biomedical applications. However, the ligand exchange process has a great effect on the PL properties of the material, such as a decrease in PLQY and blue shift in the emission position. Therefore, direct synthesis in water is preferred with postmodification with polymers and other capping agents which can improve the solubility, biocompatibility and target specificity of the material. The surface-modified CIS core and CIS/ZnS core/shell QDs have been tested in vivo and in vitro in various cell lines and animals for tumor imaging, lymph node imaging, etc., which shows the excellent applicability of the material for a clinical trial.

Even though there are various green synthesis approaches reported for the synthesis of CIS-based QDs, a complete green synthesis has not been fully established. The authors recommend a thorough research in the designing of a green synthesis protocol for CIS QDs. The tuning of optical properties by mere adjustment of the ratio between metal precursors will not be enough. Since the formation of CIS QDs also depends on other parameters such as the nature of the capping agent, concentration of the precursors, the effect of pH, the nature of shell source, and reaction temperature, a detailed optimization of parameters is required when a new precursor or capping agent is chosen. Most of the studies also reported CIS and CIS/ZnS QDs as "nontoxic", which was based on an average observation and histology. More investigations are needed in this area using different cytotoxicity assays for a concrete report on the toxicity of this material. Further studies are also required in the modification of synthetic strategies towards large scale synthesis, without any significant change in the PL properties of the material when compared to those synthesize in the laboratory.

Author Contributions: Conceptualization, R.J.V. and O.S.O.; methodology, R.J.V. and O.S.O.; validation, O.S.O.; formal analysis, R.J.V. and O.S.O.; investigation, R.J.V. and O.S.O.; resources, O.S.O.; writing—original draft preparation, R.J.V.; writing—review and editing, R.J.V. and O.S.O.; supervision, O.S.O.; project administration, O.S.O.; funding acquisition, O.S.O. All authors have read and agreed to the published version of the manuscript.

Funding: The authors would like to thank the National Research Foundation (N.R.F) under the Competitive Programmed for Rated Researchers (CPRR), grant no 106060, and the University of Johannesburg (URC) and the Faculty of Science (FRC) for financial support.

Conflicts of Interest: The authors declare no conflict of interest.

References

1. Maluleke, R.; Sakho, E.H.M.; Oluwafemi, O.S. Aqueous synthesis of glutathione-capped $CuInS_2$/ZnS quantum dots-graphene oxide nanocomposite as fluorescence "switch OFF" for explosive detection. *Mater. Lett.* **2020**. [CrossRef]
2. Jose Varghese, R.; Parani, S.; Adeyemi, O.O.; Remya, V.R.; Sakho, E.H.M.; Maluleke, R.; Thomas, S.; Oluwafemi, O.S. Green Synthesis of Sodium Alginate Capped -$CuInS_2$ Quantum Dots with Improved Fluorescence Properties. *J. Fluoresc.* **2020**. [CrossRef]
3. Jose Varghese, R.; Parani, S.; Remya, V.R.; Maluleke, R.; Thomas, S.; Oluwafemi, O.S. Sodium alginate passivated $CuInS_2$/ZnS QDs encapsulated in the mesoporous channels of amine modified SBA 15 with excellent photostability and biocompatibility. *Int. J. Biol. Macromol.* **2020**. [CrossRef] [PubMed]
4. Jawhar, N.N.; Soheyli, E.; Yazici, A.F.; Mutlugun, E.; Sahraei, R. Preparation of highly emissive and reproducible Cu–In–S/ZnS core/shell quantum dots with a mid-gap emission character. *J. Alloys Compd.* **2020**, *824*. [CrossRef]
5. Sun, G.; Xing, W.; Xing, R.; Cong, L.; Tong, S.; Yu, S. Targeting breast cancer cells with a cuins2/ZnS quantum dot-labeled Ki-67 bioprobe. *Oncol. Lett.* **2018**. [CrossRef]

6. Ranjbar-Navazi, Z.; Omidi, Y.; Eskandani, M.; Davaran, S. Cadmium-free quantum dot-based theranostics. *TrAC Trends Anal. Chem.* **2019**, *118*, 386–400. [CrossRef]
7. Allen, P.M.; Bawendi, M.G. Ternary I-III-VI quantum dots luminescent in the red to near-infrared. *J. Am. Chem. Soc.* **2008**. [CrossRef] [PubMed]
8. Pan, D.; An, L.; Sun, Z.; Hou, W.; Yang, Y.; Yang, Z.; Lu, Y. Synthesis of Cu-In-S ternary nanocrystals with tunable structure and composition. *J. Am. Chem. Soc.* **2008**. [CrossRef] [PubMed]
9. Ibáñez, M.; Zamani, R.; Li, W.; Shavel, A.; Arbiol, J.; Morante, J.R.; Cabot, A. Extending the nanocrystal synthesis control to quaternary compositions. *Cryst. Growth Des.* **2012**. [CrossRef]
10. Aldakov, D.; Lefrançois, A.; Reiss, P. Ternary and quaternary metal chalcogenide nanocrystals: Synthesis, properties and applications. *J. Mater. Chem. C* **2013**. [CrossRef]
11. Zhong, H.; Mirkovic, T.; Scholes, G.D. Nanocrystal Synthesis. In *Comprehensive Nanoscience and Technology*; Elsevier: Amsterdam, The Netherlands, 2011; pp. 153–201. ISBN 9780123743909.
12. Zamani, R.R.; Ibáez, M.; Luysberg, M.; García-Castelló, N.; Houben, L.; Prades, J.D.; Grillo, V.; Dunin-Borkowski, R.E.; Morante, J.R.; Cabot, A.; et al. Polarity-driven polytypic branching in Cu-based quaternary chalcogenide nanostructures. *ACS Nano* **2014**. [CrossRef] [PubMed]
13. Lesnyak, V.; George, C.; Genovese, A.; Prato, M.; Casu, A.; Ayyappan, S.; Scarpellini, A.; Manna, L. Alloyed copper chalcogenide nanoplatelets via partial cation exchange reactions. *ACS Nano* **2014**. [CrossRef] [PubMed]
14. Chen, Y.; Li, S.; Huang, L.; Pan, D. Green and Facile Synthesis of Water-Soluble Cu–In–S/ZnS Core/Shell Quantum Dots. *Inorg. Chem.* **2013**, *52*, 7819–7821. [CrossRef] [PubMed]
15. Mir, I.A.; Das, K.; Akhter, T.; Ranjan, R.; Patel, R.; Bohidar, H.B. Eco-friendly synthesis of $CuInS_2$ and $CuInS_2$@ZnS quantum dots and their effect on enzyme activity of lysozyme. *RSC Adv.* **2018**. [CrossRef]
16. Arshad, A.; Akram, R.; Iqbal, S.; Batool, F.; Iqbal, B.; Khalid, B.; Khan, A.U. Aqueous synthesis of tunable fluorescent, semiconductor $CuInS_2$ quantum dots for bioimaging. *Arab. J. Chem.* **2019**. [CrossRef]
17. Van Der Stam, W.; Berends, A.C.; Rabouw, F.T.; Willhammar, T.; Ke, X.; Meeldijk, J.D.; Bals, S.; De Mello Donega, C. Luminescent $CuInS_2$ quantum dots by partial cation exchange in $Cu_{2-x}S$ nanocrystals. *Chem. Mater.* **2015**, *27*, 621–628. [CrossRef]
18. Tsolekile, N.; Nahle, S.; Zikalala, N.; Parani, S.; Sakho, E.H.M.; Joubert, O.; Matoetoe, M.C.; Songca, S.P.; Oluwafemi, O.S. Cytotoxicity, fluorescence tagging and gene-expression study of CuInS/ZnS QDS - meso (hydroxyphenyl) porphyrin conjugate against human monocytic leukemia cells. *Sci. Rep.* **2020**, *10*, 1–13. [CrossRef]
19. Kolny-Olesiak, J.; Weller, H. Synthesis and application of colloidal $CuInS_2$ semiconductor nanocrystals. *ACS Appl. Mater. Interfaces* **2013**, *23*, 12221–12237.
20. Zhong, H.; Lo, S.S.; Mirkovic, T.; Li, Y.; Ding, Y.; Li, Y.; Scholes, G.D. Noninjection gram-scale synthesis of monodisperse pyramidal $CuInS_2$ nanocrystals and their size-dependent properties. *ACS Nano* **2010**. [CrossRef]
21. Zhong, H.; Zhou, Y.; Ye, M.; He, Y.; Ye, J.; He, C.; Yang, C.; Li, Y. Controlled synthesis and optical properties of colloidal ternary chalcogenide $CuInS_2$ nanocrystals. *Chem. Mater.* **2008**, *20*, 6434–6443. [CrossRef]
22. Li, T.L.; Teng, H. Solution synthesis of high-quality $CuInS_2$ quantum dots as sensitizers for TiO_2 photoelectrodes. *J. Mater. Chem.* **2010**. [CrossRef]
23. Pan, D.; Wang, X.; Zhou, Z.H.; Chen, W.; Xu, C.; Lu, Y. Synthesis of quaternary semiconductor nanocrystals with tunable band gaps. *Chem. Mater.* **2009**. [CrossRef]
24. Bozyigit, D.; Wood, V. Challenges and solutions for high-efficiency quantum dot-based LEDs. *MRS Bull.* **2013**. [CrossRef]
25. De Trizio, L.; Prato, M.; Genovese, A.; Casu, A.; Povia, M.; Simonutti, R.; Alcocer, M.J.P.; D'Andrea, C.; Tassone, F.; Manna, L. Strongly fluorescent quaternary Cu-In-Zn-S nanocrystals prepared from $Cu_{1-x}InS_2$ nanocrystals by partial cation exchange. *Chem. Mater.* **2012**. [CrossRef]
26. Zhong, H.; Bai, Z.; Zou, B. Tuning the luminescence properties of colloidal I-III-VI semiconductor nanocrystals for optoelectronics and biotechnology applications. *J. Phys. Chem. Lett.* 2012. [CrossRef]
27. Hong, G.; Antaris, A.L.; Dai, H. Near-infrared fluorophores for biomedical imaging. *Nat. Biomed. Eng.* **2017**, *1*, 1–22. [CrossRef]
28. Batabyal, S.K.; Tian, L.; Venkatram, N.; Ji, W.; Vittal, J.J. Phase-selective synthesis of $CuInS_2$ nanocrystals. *J. Phys. Chem. C* **2009**. [CrossRef]

29. Leach, A.D.P.; Mast, L.G.; Hernández-Pagán, E.A.; Macdonald, J.E. Phase dependent visible to near-infrared photoluminescence of $CuInS_2$ nanocrystals. *J. Mater. Chem. C* **2015**. [CrossRef]
30. Wang, Y.; Zhao, X.; Liu, F.; Zhang, X.; Chen, H.; Bao, F.; Liu, X. Selective synthesis of cubic and hexagonal phase of $CuInS_2$ nanocrystals by microwave irradiation. *RSC Adv.* **2014**. [CrossRef]
31. Ning, J.; Kershaw, S.V.; Rogach, A.L. Synthesis and Optical Properties of Cubic Chalcopyrite/Hexagonal Wurtzite Core/Shell Copper Indium Sulfide Nanocrystals. *J. Am. Chem. Soc.* **2019**. [CrossRef]
32. Yoshino, K.; Ikari, T.; Shirakata, S.; Miyake, H.; Hiramatsu, K. Sharp band edge photoluminescence of high-purity $CuInS_2$ single crystals. *Appl. Phys. Lett.* **2001**. [CrossRef]
33. Torimoto, T.; Adachi, T.; Okazaki, K.I.; Sakuraoka, M.; Shibayama, T.; Ohtani, B.; Kudo, A.; Kuwabata, S. Facile synthesis of ZnS-$AgInS_2$ solid solution nanoparticles for a color-adjustable luminophore. *J. Am. Chem. Soc.* **2007**. [CrossRef] [PubMed]
34. Liu, S.; Na, W.; Pang, S.; Shi, F.; Su, X. A label-free fluorescence detection strategy for lysozyme assay using $CuInS_2$ quantum dots. *Analyst* **2014**. [CrossRef]
35. Liu, Z.; Ma, Q.; Wang, X.; Lin, Z.; Zhang, H.; Liu, L.; Su, X. A novel fluorescent nanosensor for detection of heparin and heparinase based on $CuInS_2$ quantum dots. *Biosens. Bioelectron.* **2014**. [CrossRef] [PubMed]
36. Yu, Y.X.; Ouyang, W.X.; Liao, Z.T.; Du, B.B.; Zhang, W. De Construction of ZnO/ZnS/CdS/$CuInS_2$ core-shell nanowire arrays via ion exchange: P-n junction photoanode with enhanced photoelectrochemical activity under visible light. *ACS Appl. Mater. Interfaces* **2014**. [CrossRef]
37. Xiao, J.; Xie, Y.; Tang, R.; Qian, Y. Synthesis and characterization of ternary $CuInS_2$ nanorods via a hydrothermal route. *J. Solid State Chem.* **2001**. [CrossRef]
38. Castro, S.L.; Bailey, S.G.; Raffaelle, R.P.; Banger, K.K.; Hepp, A.F. Nanocrystalline chalcopyrite materials ($CuInS_2$ and $CuInSe_2$) via low-temperature pyrolysis of molecular single-source precursors. *Chem. Mater.* **2003**, *15*, 3142–3147. [CrossRef]
39. Banger, K.K.; Harris, J.D.; Cowen, J.E.; Hepp, A.F. Facile modulation of single source precursors: The synthesis and characterization of single source precursors for deposition of ternary chalcopyrite materials. *Thin Solid Films* **2002**, *403*, 390–395. [CrossRef]
40. Gardner, J.S.; Shurdha, E.; Wang, C.; Lau, L.D.; Rodriguez, R.G.; Pak, J.J. Rapid synthesis and size control of $CuInS_2$ semi-conductor nanoparticles using microwave irradiation. *J. Nanoparticle Res.* **2008**. [CrossRef]
41. Kelly, C.V.; Jin, M.H.C.; Banger, K.K.; McNatt, J.S.; Dickman, J.E.; Hepp, A.F. Parametric study on non-vacuum chemical vapor deposition of $CuInS_2$ from a single-source precursor. *Mater. Sci. Eng. B Solid-State Mater. Adv. Technol.* **2005**, *116*, 403–408. [CrossRef]
42. Xia, C.; Winckelmans, N.; Prins, P.T.; Bals, S.; Gerritsen, H.C.; De Mello Donegá, C. Near-Infrared-Emitting $CuInS_2$/ZnS Dot-in-Rod Colloidal Heteronanorods by Seeded Growth. *J. Am. Chem. Soc.* **2018**. [CrossRef] [PubMed]
43. Renuga, V.; Neela Mohan, C.; Manikandan, A. Influence of Mn^{2+} ions on both core/shell of $CuInS_2$/ZnS nanocrystals. *Mater. Res. Bull.* **2018**. [CrossRef]
44. Niyamakom, P.; Quintilla, A.; Köhler, K.; Cemernjak, M.; Ahlswede, E.; Roggan, S. Scalable synthesis of $CuInS_2$ nanocrystal inks for photovoltaic applications. *J. Mater. Chem. A* **2015**. [CrossRef]
45. Hua, J.; Cheng, H.; Yuan, X.; Zhang, Y.; Liu, M.; Meng, X.; Li, H.; Zhao, J. Photoluminescence quenching and electron transfer in $CuInS_2$/ZnS core/shell quantum dot and FePt nanoparticle blend films. *RSC Adv.* **2015**. [CrossRef]
46. Hirpo, W.; Dhingra, S.; Sutorik, A.C.; Kanatzidis, M.G. Synthesis of Mixed Copper-Indium Chalcogenolates. Single-Source Precursors for the Photovoltaic Materials $CuInQ_2$ (Q = S, Se). *J. Am. Chem. Soc.* **1993**. [CrossRef]
47. Banger, K.K.; Hollingsworth, J.A.; Harris, J.D.; Cowen, J.; Buhro, W.E.; Hepp, A.F. Ternary single-source precursors for polycrystalline thin-film solar cells. *Appl. Organomet. Chem.* **2002**. [CrossRef]
48. Nairn, J.J.; Shapiro, P.J.; Twamley, B.; Pounds, T.; Von Wandruszka, R.; Rick Fletcher, T.; Williams, M.; Wang, C.; Grant Norton, M. Preparation of ultrafine chalcopyrite nanoparticles via the photochemical decomposition of molecular single-source precursors. *Nano Lett.* **2006**, *6*, 1218–1223. [CrossRef]
49. Li, L.; Daou, T.J.; Texier, I.; Chi, T.T.K.; Liem, N.Q.; Reiss, P. Highly luminescent cuins 2/ZnS Core/Shell nanocrystals: Cadmium-free quantum dots for in vivo imaging. *Chem. Mater.* **2009**. [CrossRef]
50. Pearson, R.G. Hard and Soft Acids and Bases. *J. Am. Chem. Soc.* **1963**. [CrossRef]

51. Chetty, S.S.; Praneetha, S.; Vadivel Murugan, A.; Govarthanan, K.; Verma, R.S. Microwave-Assisted Synthesis of Quasi-Pyramidal $CuInS_2$–ZnS Nanocrystals for Enhanced Near-Infrared Targeted Fluorescent Imaging of Subcutaneous Melanoma. *Adv. Biosyst.* **2019**. [CrossRef]
52. Nose, K.; Soma, Y.; Omata, T.; Otsuka-Yao-Matsuo, S. Synthesis of ternary $CuInS_2$ nanocrystals; phase determination by complex ligand species. *Chem. Mater.* **2009**. [CrossRef]
53. Han, S.; Kong, M.; Guo, Y.; Wang, M. Synthesis of copper indium sulfide nanoparticles by solvothermal method. *Mater. Lett.* **2009**. [CrossRef]
54. Yue, W.; Han, S.; Peng, R.; Shen, W.; Geng, H.; Wu, F.; Tao, S.; Wang, M. $CuInS_2$ quantum dots synthesized by a solvothermal route and their application as effective electron acceptors for hybrid solar cells. *J. Mater. Chem.* **2010**. [CrossRef]
55. Xia, C.; Meeldijk, J.D.; Gerritsen, H.C.; De Mello Donega, C. Highly Luminescent Water-Dispersible NIR-Emitting Wurtzite $CuInS_2$/ZnS Core/Shell Colloidal Quantum Dots. *Chem. Mater.* **2017**, *29*, 4940–4951. [CrossRef]
56. su Kim, Y.; Lee, Y.; Kim, Y.; Kim, D.; Choi, H.S.; Park, J.C.; Nam, Y.S.; Jeon, D.Y. Synthesis of efficient near-infrared-emitting $CuInS_2$/ZnS quantum dots by inhibiting cation-exchange for bio application. *RSC Adv.* **2017**. [CrossRef]
57. Macdonald, T.J.; Mange, Y.J.; Dewi, M.; McFadden, A.; Skinner, W.M.; Nann, T. Cation exchange of aqueous $CuInS_2$ quantum dots. *CrystEngComm* **2014**. [CrossRef]
58. Jia, L.; Wang, Y.; Nie, Q.; Liu, B.; Liu, E.; Hu, X.; Fan, J. Aqueous-synthesis of $CuInS_2$ core and $CuInS_2$/ZnS core/shell quantum dots and their optical properties. *Mater. Lett.* **2017**. [CrossRef]
59. Tsolekile, N.; Ncapayi, V.; Parani, S.; Sakho, E.H.M.; Matoetoe, M.C.; Songca, S.P.; Oluwafemi, O.S. Synthesis of fluorescent $CuInS_2$/ZnS quantum dots - Porphyrin conjugates for photodynamic therapy. *MRS Commun.* **2018**. [CrossRef]
60. Xi, Y.; Yang, J.; Ge, Y.; Zhao, S.; Wang, J.; Li, Y.; Hao, Y.; Chen, J.; Zhu, Y. One-pot synthesis of water-soluble near-infrared fluorescence RNase A capped $CuInS_2$ quantum dots for: In vivo imaging. *RSC Adv.* **2017**. [CrossRef]
61. Chen, Y.; Li, S.; Huang, L.; Pan, D. Low-cost and gram-scale synthesis of water-soluble Cu–In–S/ZnS core/shell quantum dots in an electric pressure cooker. *Nanoscale* **2014**, *6*, 1295–1298. [CrossRef]
62. Akdas, T.; Haderlein, M.; Walter, J.; Apeleo Zubiri, B.; Spiecker, E.; Peukert, W. Continuous synthesis of $CuInS_2$ quantum dots. *RSC Adv.* **2017**. [CrossRef]
63. Wiles, C.; Watts, P. Continuous flow reactors, a tool for the modern synthetic chemist. *European J. Org. Chem.* **2008**, *2008*, 1655–1671. [CrossRef]
64. Fitzmorris, R.C.; Oleksak, R.P.; Zhou, Z.; Mangum, B.D.; Kurtin, J.N.; Herman, G.S. Structural and optical characterization of $CuInS_2$ quantum dots synthesized by microwave-assisted continuous flow methods. *J. Nanoparticle Res.* **2015**. [CrossRef]
65. Lee, J.; Han, C.S. Large-scale synthesis of highly emissive and photostable $CuInS_2$/ZnS nanocrystals through hybrid flow reactor. *Nanoscale Res. Lett.* **2014**. [CrossRef]
66. Li, S.; Chen, Y.; Huang, L.; Pan, D. Simple continuous-flow synthesis of Cu-In-Zn-S/ZnS and Ag-In-Zn-S/ZnS core/shell quantum dots. *Nanotechnology* **2013**. [CrossRef]
67. Shestopalov, I.; Tice, J.D.; Ismagilov, R.F. Multi-step synthesis of nanoparticles performed on millisecond time scale in a microfluidic droplet-based system. *Lab Chip* **2004**. [CrossRef]
68. Yashina, A.; Lignos, I.; Stavrakis, S.; Choo, J.; Demello, A.J. Scalable production of $CuInS_2$/ZnS quantum dots in a two-step droplet-based microfluidic platform. *J. Mater. Chem. C* **2016**. [CrossRef]
69. Kim, E.M.; Lim, S.T.; Sohn, M.H.; Jeong, H.J. Facile synthesis of near-infrared $CuInS_2$/ZnS quantum dots and glycol-chitosan coating for in vivo imaging. *J. Nanoparticle Res.* **2017**. [CrossRef]
70. Park, J.; Kim, S.W. $CuInS_2$/ZnS core/shell quantum dots by cation exchange and their blue-shifted photoluminescence. *J. Mater. Chem.* **2011**. [CrossRef]
71. Deng, C.; Fu, B.; Wang, Y.; Yang, L. Fabrication of Water-Soluble $CuInS_2$ Quantum Dots by Hot-Injection Method and Phase Transfer Strategy. *Nano* **2018**. [CrossRef]
72. Kim, H.; Jang, H.S.; Kwon, B.H.; Suh, M.; Kim, Y.; Cheong, S.H.; Jeon, D.Y. In situ synthesis of thiol-capped $CuInS_2$-ZnS quantum dots embedded in silica powder by sequential ligand-exchange and silanization. *Electrochem. Solid-State Lett.* **2012**. [CrossRef]

73. Zhao, C.; Bai, Z.; Liu, X.; Zhang, Y.; Zou, B.; Zhong, H. Small GSH-Capped $CuInS_2$ Quantum Dots: MPA-Assisted Aqueous Phase Transfer and Bioimaging Applications. *ACS Appl. Mater. Interfaces* **2015**. [CrossRef] [PubMed]
74. Wang, Z.; Zhang, X.; Xin, W.; Yao, D.; Liu, Y.; Zhang, L.; Liu, W.; Zhang, W.; Zheng, W.; Yang, B.; et al. Facile Synthesis of Cu-In-S/ZnS Core/Shell Quantum Dots in 1-Dodecanethiol for Efficient Light-Emitting Diodes with an External Quantum Efficiency of 7.8%. *Chem. Mater.* **2018**. [CrossRef]
75. Chuang, P.H.; Lin, C.C.; Liu, R.S. Emission-tunable $CuInS_2$/ZnS quantum dots: Structure, optical properties, and application in white light-emitting diodes with high color rendering index. *ACS Appl. Mater. Interfaces* **2014**, *6*, 15379–15387. [CrossRef]
76. Xie, R.; Rutherford, M.; Peng, X. Formation of high-quality I#III#VI semiconductor nanocrystals by tuning relative reactivity of cationic precursors. *J. Am. Chem. Soc.* **2009**, *131*, 5691–5697. [CrossRef] [PubMed]
77. Liu, S.; Zhang, H.; Qiao, Y.; Su, X. One-pot synthesis of ternary $CuInS_2$ quantum dots with near-infrared fluorescence in aqueous solution. *RSC Adv.* **2012**. [CrossRef]
78. Zhang, J.; Sun, W.; Yin, L.; Miao, X.; Zhang, D. One-pot synthesis of hydrophilic $CuInS_2$ and $CuInS_2$-ZnS colloidal quantum dots. *J. Mater. Chem. C* **2014**. [CrossRef]
79. Zhang, C.; Xia, Y.; Lian, L.; Fu, X.; Yin, L.; Zhang, J.; Luo, W.; Miao, X.; Zhang, D. Dependence of the Photoluminescence of Hydrophilic $CuInS_2$ Colloidal Quantum Dots on Cu-to-In Molar Ratios. *J. Electron. Mater.* **2019**, *48*, 286–295. [CrossRef]
80. Peng, Z.A.; Peng, X. Nearly monodisperse and shape-controlled CdSe nanocrystals via alternative routes: Nucleation and growth. *J. Am. Chem. Soc.* **2002**. [CrossRef]
81. Yuan, Y.; Riehle, F.S.; Gu, H.; Thomann, R.; Urban, G.; Krüger, M. Critical parameters for the scale-up synthesis of quantum dots. *J. Nanosci. Nanotechnol.* **2010**, *10*, 6041–6045. [CrossRef]
82. Joo, J.; Na, H.B.; Yu, T.; Yu, J.H.; Kim, Y.W.; Wu, F.; Zhang, J.Z.; Hyeon, T. Generalized and facile synthesis of semiconducting metal sulfide nanocrystals. *J. Am. Chem. Soc.* **2003**. [CrossRef]
83. Li, L.; Pandey, A.; Werder, D.J.; Khanal, B.P.; Pietryga, J.M.; Klimov, V.I. Efficient synthesis of highly luminescent copper indium sulfide-based core/shell nanocrystals with surprisingly long-lived emission. *J. Am. Chem. Soc.* **2011**, *133*, 1176–1179. [CrossRef] [PubMed]
84. Niu, G.; Ruditskiy, A.; Vara, M.; Xia, Y. Toward continuous and scalable production of colloidal nanocrystals by switching from batch to droplet reactors. *Chem. Soc. Rev.* **2015**. [CrossRef]
85. Phillips, T.W.; Lignos, I.G.; Maceiczyk, R.M.; Demello, A.J.; Demello, J.C. Nanocrystal synthesis in microfluidic reactors: Where next? *Lab Chip* **2014**. [CrossRef] [PubMed]
86. Jensen, K.F.; Reizman, B.J.; Newman, S.G. Tools for chemical synthesis in microsystems. *Lab Chip* **2014**. [CrossRef] [PubMed]
87. Kim, H.; Suh, M.; Kwon, B.H.; Jang, D.S.; Kim, S.W.; Jeon, D.Y. In situ ligand exchange of thiol-capped $CuInS_2$/ZnS quantum dots at growth stage without affecting luminescent characteristics. *J. Colloid Interface Sci.* **2011**. [CrossRef] [PubMed]
88. Tang, X.; Cheng, W.; Shi Guang Choo, E.; Xue, J. Synthesis of $CuInS_2$-ZnS alloyed nanocubes with high luminescence. *Chem. Commun.* **2011**. [CrossRef]
89. Zhang, W.; Zhong, X. Facile synthesis of ZnS-$CuInS_2$-alloyed nanocrystals for a color-tunable fluorchrome and photocatalyst. *Inorg. Chem.* **2011**. [CrossRef]
90. Zhang, J.; Xie, R.; Yang, W. A simple route for highly luminescent quaternary Cu-Zn-In-S nanocrystal emitters. *Chem. Mater.* **2011**. [CrossRef]
91. Uehara, M.; Watanabe, K.; Tajiri, Y.; Nakamura, H.; Maeda, H. Synthesis of $CuInS_2$ fluorescent nanocrystals and enhancement of fluorescence by controlling crystal defect. *J. Chem. Phys.* **2008**, *129*. [CrossRef]
92. Chen, B.; Zhong, H.; Zhang, W.; Tan, Z.; Li, Y.; Yu, C.; Zhai, T.; Bando, Y.; Yang, S.; Zou, B. Highly emissive and color-tunable $CuInS_2$-based colloidal semiconductor nanocrystals: Off-stoichiometry effects and improved electroluminescence performance. *Adv. Funct. Mater.* **2012**, *22*, 2081–2088. [CrossRef]
93. Yamamoto, T.; Luck, I.V.; Scheer, R.; Katayama-Yoshida, H. Differences in the electronic structure and compensation mechanism between n-type Zn- and Cd-doped $CuInS_2$ crystals. *Phys. B Condens. Matter* **1999**. [CrossRef]
94. Zhang, S.; Wei, S.H.; Zunger, A.; Katayama-Yoshida, H. Defect physics of the chalcopyrite semiconductor. *Phys. Rev. B Condens. Matter Mater. Phys.* **1998**. [CrossRef]

95. Philip, R.R.; Pradeep, B. Structural analysis and optical and electrical characterization of the ordered defect compound $CuIn_5Se_8$. *Semicond. Sci. Technol.* **2003**. [CrossRef]
96. Fuhr, A.S.; Yun, H.J.; Makarov, N.S.; Li, H.; McDaniel, H.; Klimov, V.I. Light Emission Mechanisms in $CuInS_2$ Quantum Dots Evaluated by Spectral Electrochemistry. *ACS Photonics* **2017**. [CrossRef]
97. Zhang, B.; Wang, Y.; Yang, C.; Hu, S.; Gao, Y.; Zhang, Y.; Wang, Y.; Demir, H.V.; Liu, L.; Yong, K.T. The composition effect on the optical properties of aqueous synthesized Cu-In-S and Zn-Cu-In-S quantum dot nanocrystals. *Phys. Chem. Chem. Phys.* **2015**. [CrossRef]
98. Hamanaka, Y.; Kuzuya, T.; Sofue, T.; Kino, T.; Ito, K.; Sumiyama, K. Defect-induced photoluminescence and third-order nonlinear optical response of chemically synthesized chalcopyrite $CuInS_2$ nanoparticles. *Chem. Phys. Lett.* **2008**. [CrossRef]
99. Tsolekile, N.; Parani, S.; Vuyelwa, N.; Maluleke, R.; Matoetoe, M.; Songca, S.; Oluwafemi, O.S. Synthesis, structural and fluorescence optimization of ternary Cu–In–S quantum dots passivated with ZnS. *J. Lumin.* **2020**. [CrossRef]
100. Ma, J.; Liu, M.; Li, Z.; Li, L. Synthesis of highly photo-stable $CuInS_2$/ZnS core/shell quantum dots. *Opt. Mater.* **2015**. [CrossRef]
101. Kays, J.C.; Saeboe, A.M.; Toufanian, R.; Kurant, D.E.; Dennis, A.M. Shell-Free Copper Indium Sulfide Quantum Dots Induce Toxicity in Vitro and in Vivo. *Nano Lett.* **2020**. [CrossRef]
102. Pons, T.; Pic, E.; Lequeux, N.; Cassette, E.; Bezdetnaya, L.; Guillemin, F.; Marchal, F.; Dubertret, B. Cadmium-free $CuInS_2$/ZnS quantum dots for sentinel lymph node imaging with reduced toxicity. *ACS Nano* **2010**, *4*, 2531–2538. [CrossRef] [PubMed]
103. Zhang, C.; Qu, G.; Sun, Y.; Wu, X.; Yao, Z.; Guo, Q.; Ding, Q.; Yuan, S.; Shen, Z.; Ping, Q.; et al. Pharmacokinetics, biodistribution, efficacy and safety of N-octyl-O-sulfate chitosan micelles loaded with paclitaxel. *Biomaterials* **2008**. [CrossRef] [PubMed]
104. Bhattarai, N.; Gunn, J.; Zhang, M. Chitosan-based hydrogels for controlled, localized drug delivery. *Adv. Drug Deliv. Rev.* **2010**, *62*, 83–99. [CrossRef] [PubMed]
105. Deng, D.; Chen, Y.; Cao, J.; Tian, J.; Qian, Z.; Achilefu, S.; Gu, Y. High-quality $CuInS_2$/ZnS quantum dots for in vitro and in vivo bioimaging. *Chem. Mater.* **2012**. [CrossRef]
106. Chen, C.W.; Wu, D.Y.; Chan, Y.C.; Lin, C.C.; Chung, P.H.; Hsiao, M.; Liu, R.S. Evaluations of the chemical stability and cytotoxicity of $CuInS_2$ and $CuInS_2$/ZnS core/shell quantum dots. *J. Phys. Chem. C* **2015**. [CrossRef]
107. Gerion, D.; Pinaud, F.; Williams, S.C.; Parak, W.J.; Zanchet, D.; Weiss, S.; Alivisatos, A.P. Synthesis and properties of biocompatible water-soluble silica-coated CdSe/ZnS semiconductor quantum dots. *J. Phys. Chem. B* **2001**. [CrossRef]
108. Hsu, J.C.; Huang, C.C.; Ou, K.L.; Lu, N.; Mai, F.D.; Chen, J.K.; Chang, J.Y. Silica nanohybrids integrated with $CuInS_2$/ZnS quantum dots and magnetite nanocrystals: Multifunctional agents for dual-modality imaging and drug delivery. *J. Mater. Chem.* **2011**. [CrossRef]
109. Foda, M.F.; Huang, L.; Shao, F.; Han, H.Y. Biocompatible and highly luminescent near-infrared $CuInS_2$/ZnS quantum dots embedded silica beads for cancer cell imaging. *ACS Appl. Mater. Interfaces* **2014**. [CrossRef]
110. Varghese, J.; Sakthipriya, P.; Rachel, G.; Ananthi, N. Polylactic acid coated SBA-15 functionalized with 3-aminopropyl triethoxysilane. *Indian J. Chem. Sect. A Inorganic Phys. Theor. Anal. Chem.* **2017**, *56A*, 621–625.
111. Liu, Z.; Chen, N.; Dong, C.; Li, W.; Guo, W.; Wang, H.; Wang, S.; Tan, J.; Tu, Y.; Chang, J. Facile Construction of Near Infrared Fluorescence Nanoprobe with Amphiphilic Protein-Polymer Bioconjugate for Targeted Cell Imaging. *ACS Appl. Mater. Interfaces* **2015**. [CrossRef]
112. Sharma, V.K.; Gokyar, S.; Kelestemur, Y.; Erdem, T.; Unal, E.; Demir, H.V. Manganese doped fluorescent paramagnetic nanocrystals for dual-modal imaging. *Small* **2014**. [CrossRef] [PubMed]
113. Smith, A.M.; Nie, S. Bright and compact alloyed quantum dots with broadly tunable near-infrared absorption and fluorescence spectra through mercury cation exchange. *J. Am. Chem. Soc.* **2011**. [CrossRef]
114. Ma, Q.; Su, X. Near-infrared quantum dots: Synthesis, functionalization and analytical applications. *Analyst* **2010**, *135*, 1867–1877. [CrossRef] [PubMed]
115. Shen, J.; Li, Y.; Zhu, Y.; Yang, X.; Yao, X.; Li, J.; Huang, G.; Li, C. Multifunctional gadolinium-labeled silica-coated Fe_3O_4 and $CuInS_2$ nanoparticles as a platform for in vivo tri-modality magnetic resonance and fluorescence imaging. *J. Mater. Chem. B* **2015**. [CrossRef] [PubMed]

116. Zhang, J.; Hao, G.; Yao, C.; Hu, S.; Hu, C.; Zhang, B. Paramagnetic albumin decorated $CuInS_2$/ZnS QDs for CD133+ glioma bimodal MR/fluorescence targeted imaging. *J. Mater. Chem. B* **2016**. [CrossRef]
117. Tsolekile, N.; Ncapayi, V.; Obiyenwa, G.K.; Matoetoe, M.; Songca, S.; Oluwafemi, O.S. Synthesis of meso-tetra-(4-sulfonatophenyl) porphyrin (TPPS4)—CuInS/ZnS quantum dots conjugate as an improved photosensitizer. *Int. J. Nanomed.* **2019**. [CrossRef]